Scheme 1. Synthetic Route for BAP-1[a]

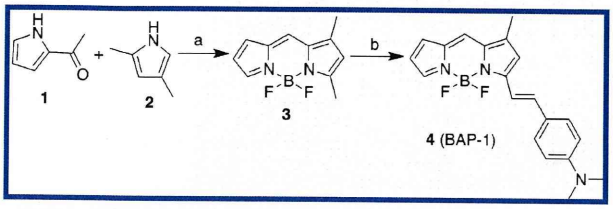

[a]Reagents: (a) $CHCl_3$, $POCl_3$, BF_3OEt_2, Et_3N; (b) toluene, 4-dimethylaminobenzaldehyde, piperidine, and AcOH.

First, we evaluated the fluorescent properties including absorption, excitation, emission wavelength, and quantum yield of BAP-1 in $CHCl_3$. BAP-1 exhibited absorption, excitation, and emission wavelengths of 604, 614, and 648 nm, respectively, with a high fluorescent quantum yield (46.8%) (Table 1). Although

Table 1. Fluorescence Characterization of BAP-1[a]

Abs (nm)	Ex (nm)	Em (nm)	quantum yield (%)
604	614	648	46.8

[a]Absorbance, fluorescence excitation and emission, and quantum yield of BAP-1 were determined with 10 μM of the compound in $CHCl_3$.

BAP-1 showed slightly shorter wavelengths of excitation/emission at 614/648 nm than are appropriate for optical imaging in vivo, its high quantum yield was expected to enable the imaging of Aβ plaques in shallow areas of the mouse brain.

Furthermore, when BAP-1 existed in a solution containing Aβ aggregates or bovine serum albumin (BSA), its fluorescent intensity increased with the concentration of the aggregates, indicating affinity for Aβ aggregates (Figure 1). However, we

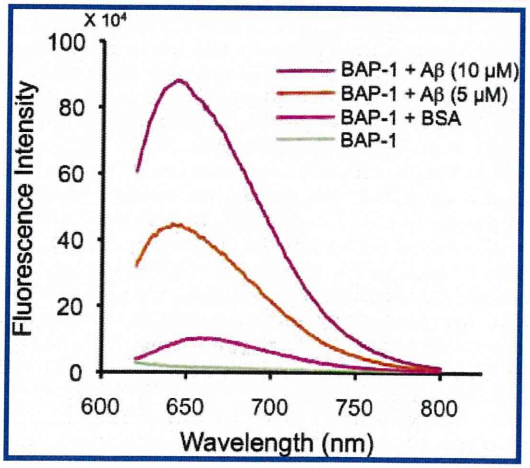

Figure 1. Fluorescence intensity of BAP-1 upon interaction with Aβ42 aggregates and BSA.

found no significant change in fluorescence during the incubation with BSA, indicating that there is little interaction between BAP-1 and BSA.

To quantify the affinity for Aβ aggregates, we measured the apparent binding constant (K_d) of BAP-1 by conducting a saturation assay (Figure 2). The fluorescent intensity of BAP-1 increased in a dose-dependent manner and was saturated at the higher concentration. Transformation of the saturation binding data to Scatchard plots provided linear plots, indicating that

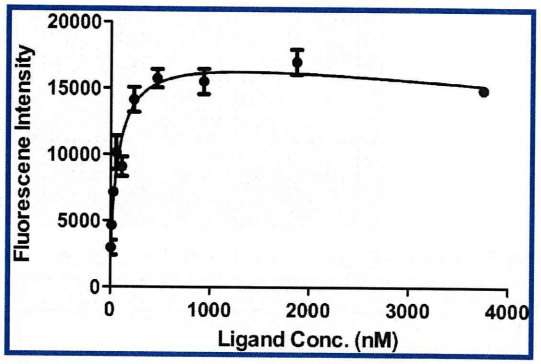

Figure 2. Plot of the fluorescence intensity (Em = 673 nm) as a function of the concentration of BAP-1 in the presence of Aβ42 aggregates (2.2 μM) in solutions.

BAP-1 has one binding site on Aβ aggregates. BAP-1 showed excellent affinity for Aβ aggregates at a K_d value of 44.1 nM.

To confirm the affinity of BAP-1 for Aβ plaques in the brain, neuropathological fluorescent staining with BAP-1 was carried out using brain sections from Tg2576 mice (Figure 3). Tg2576 mice have been specifically engineered to overproduce Aβ plaques in the brain[48] and frequently used to evaluate the specific binding of Aβ plaques in experiments in vitro and in vivo.[49−51] Many fluorescent spots were observed in the brain sections of Tg2576 mice (32-month-old, female) (Figure 3A), while no spots were observed in the wild-type mice (29-month-old, female) (Figure 3B). The staining pattern was consist with that observed with thioflavin S (Figure 3C), a dye commonly used to stain Aβ plaques,[52] indicating that BAP-1 shows specific binding to Aβ plaques in the mouse brain.

One important prerequisite for a probe for imaging of Aβ plaques in the brain is to penetrate the blood−brain barrier after an i.v. injection. Furthermore, the ideal amyloid-imaging agent should be rapidly washed out from normal brain tissue in addition to having a high brain uptake. Since normal brain tissue has no amyloid plaques to trap the agent, the washout should be fast, providing a higher signal-to-noise ratio in the AD brain. To test the uptake into and washout from the brain, we determined the fluorescent intensity in the brain after the injection of BAP-1 into a normal mouse. BAP-1 showed high initial brain uptake at 2 min postinjection, but the fluorescence that accumulated in the brain was rapidly eliminated, both of which are highly desirable properties for Aβ imaging probes (Figure 4).

To evaluate the potential of BAP-1 in living brain tissue, we carried out experiments ex vivo using a Tg2576 mouse (25-month-old male) and a wild-type mouse (25-month-old male) as an age-matched control. The fluorescence in whole brains removed at 1 h postinjection of BAP-1 was much higher in the Tg2576 mouse than wild-type mouse (Figure 5).

To further evaluate what the higher fluorescence in the Tg2576 mouse brain was derived from, we prepared frozen sections from both brains and observed them with a fluorescence microscope. The brain sections from the Tg2576 mouse showed distinctive staining of Aβ plaques by BAP-1 (Figure 6A), while those from the wild-type mouse showed no such staining (Figure 6B). The staining pattern in the brain sections from the Tg2576 mouse was consistent with that observed on immunohistochemical staining with an antibody specific for Aβ(1−42) (BC05) as shown by arrows in Figure 6C. The results suggest that BAP-1 penetrated the blood−brain

dx.doi.org/10.1021/cn3000058 | ACS Chem. Neurosci. 2012, 3, 319−324

Figure 3. Neuropathological staining of BAP-1 in a 10-μm section from a Tg2576 mouse brain (A) and a wild-type mouse brain (B). Labeled plaques were confirmed by staining of the adjacent section with thioflavin-S (C).

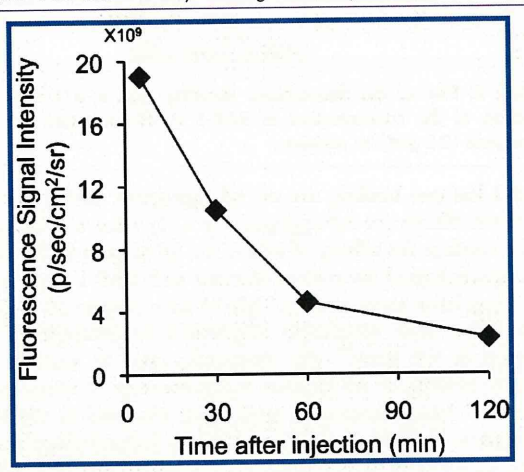

Figure 4. Fluorescence intensity after injection of BAP-1 into ddY mice with an IVIS spectrum.

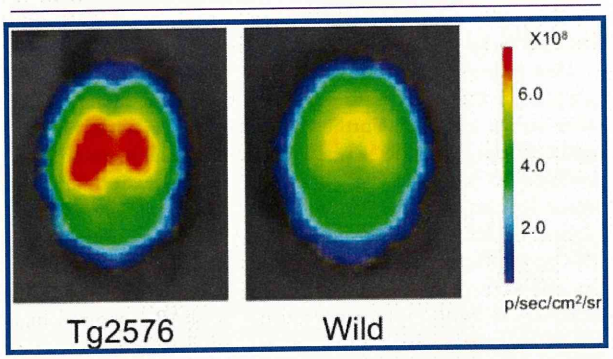

Figure 5. Comparison of the fluorescence intensity in the brain after the injection of BAP-1 into a Tg2576 mouse (A) and wild-type mouse (B).

barrier and selectively labeled the Aβ plaques in the brain, as reflected by the biodistribution experiments and in vitro binding assays. To our knowledge, this is the first report that BODIPY-based probes can function as Aβ imaging probes in vivo. However, the excitation and emission wavelengths of BAP-1 were still shorter than the ideal wavelengths for optical imaging in vivo. Several BODIPY derivatives with longer wavelengths in the near-infrared region have recently been reported.[53−55] On the basis of these findings, we may develop more appropriate BODIPY-based probes for the imaging of Aβ plaques in vivo.

We also conducted in vivo imaging experiments using Tg2576 mice and age-matched controls. However, we could not find a significant difference between the two groups, because the fluorescence of BAP-1 accumulated nonspecifically in the scalp in both groups. To improve nonspecific accumulation in the scalp, further modification of the BODIPY scaffold will be needed in the future.

In conclusion, we successfully designed and synthesized a BODIPY-based Aβ probe, BAP-1, for optical imaging in vivo. In binding experiments in vitro, BAP-1 showed high affinity for Aβ aggregates. BAP-1 clearly stained Aβ plaques in the mouse brain, reflecting its affinity for Aβ aggregates in vitro. In animal experiments using normal mice, BAP-1 displayed good uptake into and fast washout from the brain. In addition, ex vivo fluorescent staining of brain sections from Tg2576 mice after the injection of BAP-1 showed selective binding of Aβ plaques with little nonspecific binding. These findings suggest BAP-1 to be a useful molecular probe for the detection of Aβ plaques in AD brains and also provide useful information for the development of new BODIPY-based probes in the future.

METHODS

General. All reagents were obtained commercially and used without further purification unless otherwise indicated. ^{1}H and ^{13}C NMR spectra were obtained on a JEOL JNM-LM400 spectrometer with TMS as an internal standard. Coupling constants are reported in hertz. Multiplicity was defined by s (singlet), d (doublet), and m (multiplet). Mass spectra were obtained on a SHIMADZU GC-2010. HPLC was performed with a Shimadzu system (a LC-20AD pump with a SPD-20A UV detector, λ = 254 nm) using a Cosmosil C18 column (Nacalai Tesque, 5C_{18}-AR-II, 4.6 × 150 mm) and acetonitrile/water (3/2) as the mobile phase at a flow rate of 1.0 mL/min. The target compound was proven by this method to show >95% purity.

Chemistry. *1,3-Dimethyl-4,4-difluoro-4-bora-3a,4a-diaza-s-indacene (3).* A solution of pyrrole 2-carboxyaldehyde (**1**) (368 mg, 3.87 mmol) and 2,4-dimethylpyrrole (**2**) (368 mg, 3.87 mmol) in $CHCl_3$ (10 mL) was cooled to 0 °C. After $POCl_3$ (360 μL) was added with caution, the mixture was stirred at room temperature for 2 h. BF_3·OEt_2 (3 mL) and Et_3N (3 mL) were added sequentially, and the resulting mixture was stirred at room temperature for 10 min. The solution was washed with H_2O and dried with Na_2SO_4. The solvent was removed, and the residue was purified by silica gel column chromatography (hexane/ethyl acetate = 2:1) to give 308 mg of **3** (36.1%). ^{1}H NMR (400 MHz, $CDCl_3$) δ 2.28 (s, 3H), 2.59 (s, 3H), 6.16 (s, 1H), 6.43 (m, 1H), 6.93 (d, J = 3.6 Hz, 1H), 7.20 (s, 1H), 7.65 (s, 1H). ^{13}C NMR (100 MHz, $CDCl_3$) δ 11.3, 15.0, 116.2, 121.2, 124.8, 126.5, 132.5, 136.5, 138.9, 146.0, 163.1. MS m/z 220 (M^+).

4,4-Difluoro-3-{(E)-{2-(4-dimethylaminophenyl)ethenyl}}-1-methyl-4-bora-3a,4a-diaza-s-indacene (4, BAP-1). Compound **3** (120 mg, 0.55 mmol) and 4-dimethylaminobenzaldehyde (82 mg, 0.55 mmol) were dissolved in toluene (10 mL) with piperidine (350 μL) and AcOH (350 μL). The mixture was stirred under reflux for 1 h. After the mixture cooled to room temperature, H_2O was added and extracted with ethyl acetate. The organic phase was dried over Na_2SO_4 and filtered. The solvent was removed, and the residue was purified by silica gel chromatography (hexane/ethyl acetate = 1:2) to give 97 mg of **4** (50.6%). ^{1}H NMR (400 MHz, $CDCl_3$) δ 2.30 (s, 3H), 3.09 (s, 6H), 6.42 (m, 1H), 6.73 (m, 3H), 6.84 (d, J = 3.9 Hz, 1H), 7.06 (s, 1H), 7.36 (d, J = 16.6 Hz, 1H), 7.46 (d, J = 16.3 Hz, 1H), 7.54 (d, J = 8.8 Hz, 2H), 7.60 (s, 1H). ^{13}C NMR (100 MHz, $CDCl_3$) δ 11.4, 40.1,

Figure 6. Ex vivo fluorescence observation of brain sections from a Tg2576 mouse (A) and wild-type mouse (B) after an injection of BAP-1. The presence of Aβ plaques in the section from the Tg2576 mouse was confirmed with immunohistochemical staining using a monoclonal Aβ antibody (C). Arrows show Aβ plaques stained by both BAP-1 (A) and immunohistochemical labeling (C).

111.9, 113.4, 115.2, 117.4, 120.4, 123.4, 123.8, 130.1, 132.6, 136.2, 138.4, 141.9, 144.4, 151.7, 160.6. MS m/z 351 (M^+).

Fluorescence Measurements Using Aβ(1−42) and BSA. A solid form of Aβ(1−42) was purchased from Peptide Institute (Osaka, Japan). Aggregation was carried out by gently dissolving the peptide (0.25 mg/mL) in PBS (pH 7.4). The solution was incubated at 37 °C for 42 h with gentle and constant shaking. A mixture (100 μM of 10% EtOH) containing BAP-1 (10 μM) and Aβ(1−42) aggregates (0, 5, and 10 μM) or BSA (45 μg/mL) was incubated at room temperature for 30 min. After incubation, fluorescence emission spectra were collected between 645 and 800 nm with excitation at 614 nm.

Measurement of the Constant for Binding of Aβ Aggregates in Vitro. A mixture (100 μL of 10% EtOH) containing BAP-1 (final conc. 0−3.75 μM) and Aβ(1−42) aggregates (final conc. 2.2 μM) or BSA (10 μM) was incubated at room temperature for 30 min. Fluorescence intensity at 673 nm was recorded (Ex: 614 nm). The K_d binding curve was generated by GraphPad Prism 5.0 (GraphPad Software, Inc., La Jolla, CA, USA).

In Vitro Fluorescent Staining of Mouse Brain Sections. The experiments with animals were conducted in accordance with our institutional guidelines and approved by the Kyoto University Animal Care Committee. The Tg2576 transgenic mouse (female, 32-month-old) and wild-type mouse (female, 29-month-old) were used as the AD model. After the mouse was sacrificed by decapitation, the brain was removed and sliced into serial sections 10 μm thick. Each slide was incubated with a 50% EtOH solution of BAP-1 (100 μM). Finally, the sections were washed in 50% EtOH for 1 min two times and examined using a microscope (BIOREVO BZ-9000, Keyence Corp., Osaka, Japan) equipped with a Texas Red filter set (excitation filter, Ex 540−580 nm; diachronic mirror, DM 595; barrier filter, BA 600−660). Thereafter, the serial sections were also stained with thioflavin S, a pathological dye commonly used for staining Aβ plaques in the brain, and examined using a microscope equipped with a GFP-BP filter set (excitation filter, Ex 450−490; diachronic mirror, DM 495; barrier filter, BA 510−560).

Ex Vivo Imaging of Brains from Normal Mice. A mixed solution consisting of 20% DMSO and 80% propylene glycol (100 μL) of BAP-1 (500 μM) was injected intravenously directly into the tail of ddY mice (5-week-old). The mice were sacrificed at 2, 10, 30, and 60 min postinjection. The brain was removed and weighed, and fluorescence images of brains were acquired with an IVIS SPECTRUM imaging system (Caliper Life Sciences Inc., Hopkinton, MA, USA) with a 0.1-s exposure (f-stop = 2) and a customized filter set (excitation, 605 nm; emission, 660 nm). The fluorescence intensity in each region of interest covering an entire tissue was expressed as photons/sec per g after the subtraction of background signals obtained in a region of interest set over an area without any tissue.

Ex Vivo Imaging Using a Tg2576 Mouse and an Age-Matched Control. A 25-month-old Tg2576 mouse and a wild-type mouse were intravenously injected with 200 μL of BAP-1 (133 μM, 10% EtOH). After 1 h, the mice were sacrificed, and the brain was removed and frozen in powdered dry ice. Fluorescence images of the brains were acquired with an IVIS SPECTRUM imaging system (Caliper Life Sciences Inc., Hopkinton, MA, USA) with a 0.1-s exposure (f-stop = 2) and a customized filter set (excitation, 605 nm; emission, 660 nm). The frozen blocks were sliced into serial sections, 20 μm thick, and examined using a microscope equipped with a Texas Red filter set. Thereafter, the presence and distribution of plaques in the same sections were confirmed with immunohistochemical staining using a monoclonal Aβ antibody (BC05) (Wako Pure Chemical Industries, Ltd., Osaka, Japan).

■ ASSOCIATED CONTENT

Supporting Information

Data for ^{1}H and ^{13}C NMR spectra and HPLC analyses of BAP-1. This material is available free of charge via the Internet at http://pubs.acs.org.

■ AUTHOR INFORMATION

Corresponding Author

*Phone: +81-75-753-4608. Fax: +81-75-753-4568. E-mail: ono@pharm.kyoto-u.ac.jp.

Author Contributions

M.O. and H.S. designed all experiments. H.W. performed the synthetic chemistry work and in vitro and in vivo experiments. H.K. performed the synthetic chemistry work.

Funding

This study was supported by the Funding Program for Next Generation World-Leading Researchers (NEXT Program) from the Japan Society for the Promotion of Science (JSPS), Japan.

Notes

The authors declare no competing financial interest.

■ ACKNOWLEDGMENTS

We thank Ms. Manami Ishikawa for helping with the synthesis of BAP-1 and Dr. Yoichi Shimizu for helping with the imaging in vivo.

■ REFERENCES

(1) Klunk, W. E. (1998) Biological markers of Alzheimer's disease. *Neurobiol. Aging 19*, 145−147.

(2) Selkoe, D. J. (2000) Imaging Alzheimer's amyloid. *Nat. Biotechnol. 18*, 823−824.

(3) Ono, M., Wilson, A., Nobrega, J., Westaway, D., Verhoeff, P., Zhuang, Z. P., Kung, M. P., and Kung, H. F. (2003) ^{11}C-labeled stilbene derivatives as Aβ-aggregate-specific PET imaging agents for Alzheimer's disease. *Nucl. Med. Biol. 30*, 565−571.

(4) Verhoeff, N. P., Wilson, A. A., Takeshita, S., Trop, L., Hussey, D., Singh, K., Kung, H. F., Kung, M. P., and Houle, S. (2004) In-vivo imaging of Alzheimer disease β-amyloid with [^{11}C]SB-13 PET. *Am. J. Geriatr. Psychiatry 12*, 584−595.

(5) Mathis, C. A., Wang, Y., Holt, D. P., Huang, G. F., Debnath, M. L., and Klunk, W. E. (2003) Synthesis and evaluation of ^{11}C-labeled 6-substituted 2-arylbenzothiazoles as amyloid imaging agents. *J. Med. Chem. 46*, 2740−2754.

(6) Klunk, W. E., Engler, H., Nordberg, A., Wang, Y., Blomqvist, G., Holt, D. P., Bergstrom, M., Savitcheva, I., Huang, G. F., Estrada, S., Ausen, B., Debnath, M. L., Barletta, J., Price, J. C., Sandell, J., Lopresti, B. J., Wall, A., Koivisto, P., Antoni, G., Mathis, C. A., and Langstrom, B. (2004) Imaging brain amyloid in Alzheimer's disease with Pittsburgh Compound-B. *Ann. Neurol. 55*, 306–319.

(7) Kudo, Y., Okamura, N., Furumoto, S., Tashiro, M., Furukawa, K., Maruyama, M., Itoh, M., Iwata, R., Yanai, K., and Arai, H. (2007) 2-(2-[2-Dimethylaminothiazol-5-yl]ethenyl)-6-(2-[fluoro]ethoxy)-benzoxazole: a novel PET agent for in vivo detection of dense amyloid plaques in Alzheimer's disease patients. *J. Nucl. Med. 48*, 553–561.

(8) Johnson, A. E., Jeppsson, F., Sandell, J., Wensbo, D., Neelissen, J. A., Jureus, A., Strom, P., Norman, H., Farde, L., and Svensson, S. P. (2009) AZD2184: a radioligand for sensitive detection of β-amyloid deposits. *J. Neurochem. 108*, 1177–1186.

(9) Swahn, B. M., Wensbo, D., Sandell, J., Sohn, D., Slivo, C., Pyring, D., Malmstrom, J., Arzel, E., Vallin, M., Bergh, M., Jeppsson, F., Johnson, A. E., Jureus, A., Neelissen, J., and Svensson, S. (2010) Synthesis and evaluation of 2-pyridylbenzothiazole, 2-pyridylbenzoxazole and 2-pyridylbenzofuran derivatives as ^{11}C-PET imaging agents for β-amyloid plaques. *Bioorg. Med. Chem. Lett. 20*, 1976–1980.

(10) Agdeppa, E. D., Kepe, V., Liu, J., Flores-Torres, S., Satyamurthy, N., Petric, A., Cole, G. M., Small, G. W., Huang, S. C., and Barrio, J. R. (2001) Binding characteristics of radiofluorinated 6-dialkylamino-2-naphthylethylidene derivatives as positron emission tomography imaging probes for β-amyloid plaques in Alzheimer's disease. *J. Neurosci. 21*, RC189.

(11) Shoghi-Jadid, K., Small, G. W., Agdeppa, E. D., Kepe, V., Ercoli, L. M., Siddarth, P., Read, S., Satyamurthy, N., Petric, A., Huang, S. C., and Barrio, J. R. (2002) Localization of neurofibrillary tangles and β-amyloid plaques in the brains of living patients with Alzheimer disease. *Am. J. Geriatr. Psychiatry 10*, 24–35.

(12) Koole, M., Lewis, D. M., Buckley, C., Nelissen, N., Vandenbulcke, M., Brooks, D. J., Vandenberghe, R., and Van Laere, K. (2009) Whole-body biodistribution and radiation dosimetry of ^{18}F-GE067: a radioligand for in vivo brain amyloid imaging. *J. Nucl. Med. 50*, 818–822.

(13) Vandenberghe, R., Van Laere, K., Ivanoiu, A., Salmon, E., Bastin, C., Triau, E., Hasselbalch, S., Law, I., Andersen, A., Korner, A., Minthon, L., Garraux, G., Nelissen, N., Bormans, G., Buckley, C., Owenius, R., Thurfjell, L., Farrar, G., and Brooks, D. J. (2010) ^{18}F-flutemetamol amyloid imaging in Alzheimer disease and mild cognitive impairment: a phase 2 trial. *Ann. Neurol. 68*, 319–329.

(14) Nelissen, N., Van Laere, K., Thurfjell, L., Owenius, R., Vandenbulcke, M., Koole, M., Bormans, G., Brooks, D. J., and Vandenberghe, R. (2009) Phase 1 study of the Pittsburgh compound B derivative ^{18}F-flutemetamol in healthy volunteers and patients with probable Alzheimer disease. *J. Nucl. Med. 50*, 1251–1259.

(15) Zhang, W., Oya, S., Kung, M. P., Hou, C., Maier, D. L., and Kung, H. F. (2005) F-18 polyethyleneglycol stilbenes as PET imaging agents targeting Aβ aggregates in the brain. *Nucl. Med. Biol. 32*, 799–809.

(16) Rowe, C. C., Ackerman, U., Browne, W., Mulligan, R., Pike, K. L., O'Keefe, G., Tochon-Danguy, H., Chan, G., Berlangieri, S. U., Jones, G., Dickinson-Rowe, K. L., Kung, H. P., Zhang, W., Kung, M. P., Skovronsky, D., Dyrks, T., Holl, G., Krause, S., Friebe, M., Lehman, L., Lindemann, S., Dinkelborg, L. M., Masters, C. L., and Villemagne, V. L. (2008) Imaging of amyloid β in Alzheimer's disease with ^{18}F-BAY94–9172, a novel PET tracer: proof of mechanism. *Lancet Neurol. 7*, 129–135.

(17) O'Keefe, G. J., Saunder, T. H., Ng, S., Ackerman, U., Tochon-Danguy, H. J., Chan, J. G., Gong, S., Dyrks, T., Lindemann, S., Holl, G., Dinkelborg, L., Villemagne, V., and Rowe, C. C. (2009) Radiation dosimetry of β-amyloid tracers ^{11}C-PiB and ^{18}F-BAY94–9172. *J. Nucl. Med. 50*, 309–315.

(18) Zhang, W., Oya, S., Kung, M. P., Hou, C., Maier, D. L., and Kung, H. F. (2005) F-18 stilbenes as PET imaging agents for detecting β-amyloid plaques in the brain. *J. Med. Chem. 48*, 5980–5988.

(19) Choi, S. R., Golding, G., Zhuang, Z., Zhang, W., Lim, N., Hefti, F., Benedum, T. E., Kilbourn, M. R., Skovronsky, D., and Kung, H. F. (2009) Preclinical properties of ^{18}F-AV-45: a PET agent for Aβ plaques in the brain. *J. Nucl. Med. 50*, 1887–1894.

(20) Wong, D. F., Rosenberg, P. B., Zhou, Y., Kumar, A., Raymont, V., Ravert, H. T., Dannals, R. F., Nandi, A., Brasic, J. R., Ye, W., Hilton, J., Lyketsos, C., Kung, H. F., Joshi, A. D., Skovronsky, D. M., and Pontecorvo, M. J. (2010) In vivo imaging of amyloid deposition in Alzheimer disease using the radioligand ^{18}F-AV-45 (flobetapir F 18). *J. Nucl. Med. 51*, 913–920.

(21) Kung, H. F., Choi, S. R., Qu, W., Zhang, W., and Skovronsky, D. (2010) ^{18}F stilbenes and styrylpyridines for PET imaging of Aβ plaques in Alzheimer's disease: a miniperspective. *J. Med. Chem. 53*, 933–941.

(22) Zhuang, Z. P., Kung, M. P., Wilson, A., Lee, C. W., Plossl, K., Hou, C., Holtzman, D. M., and Kung, H. F. (2003) Structure-activity relationship of imidazo[1,2-a]pyridines as ligands for detecting β-amyloid plaques in the brain. *J. Med. Chem. 46*, 237–243.

(23) Newberg, A. B., Wintering, N. A., Clark, C. M., Plossl, K., Skovronsky, D., Seibyl, J. P., Kung, M. P., and Kung, H. F. (2006) Use of ^{123}I IMPY SPECT to differentiate Alzheimer's disease from controls. *J. Nucl. Med. 47*, 78P.

(24) Maya, Y., Ono, M., Watanabe, H., Haratake, M., Saji, H., and Nakayama, M. (2009) Novel radioiodinated aurones as probes for SPECT imaging of β-amyloid plaques in the brain. *Bioconjugate Chem. 20*, 95–101.

(25) Sato, K., Higuchi, M., Iwata, N., Saido, T. C., and Sasamoto, K. (2004) Fluoro-substituted and ^{13}C-labeled styrylbenzene derivatives for detecting brain amyloid plaques. *Eur. J. Med. Chem. 39*, 573–578.

(26) Higuchi, M., Iwata, N., Matsuba, Y., Sato, K., Sasamoto, K., and Saido, T. C. (2005) ^{19}F and ^{1}H MRI detection of amyloid β plaques in vivo. *Nat. Neurosci. 8*, 527–533.

(27) Amatsubo, T., Yanagisawa, D., Morikawa, S., Taguchi, H., and Tooyama, I. (2010) Amyloid imaging using high-field magnetic resonance. *Magn. Reson. Med. Sci. 9*, 95–99.

(28) Yanagisawa, D., Amatsubo, T., Morikawa, S., Taguchi, H., Urushitani, M., Shirai, N., Hirao, K., Shiino, A., Inubushi, T., and Tooyama, I. (2011) In vivo detection of amyloid β deposition using ^{19}F magnetic resonance imaging with a ^{19}F-containing curcumin derivative in a mouse model of Alzheimer's disease. *Neuroscience 184*, 120–127.

(29) Hintersteiner, M., Enz, A., Frey, P., Jaton, A. L., Kinzy, W., Kneuer, R., Neumann, U., Rudin, M., Staufenbiel, M., Stoeckli, M., Wiederhold, K. H., and Gremlich, H. U. (2005) In vivo detection of amyloid-β deposits by near-infrared imaging using an oxazine-derivative probe. *Nat. Biotechnol. 23*, 577–583.

(30) Nesterov, E. E., Skoch, J., Hyman, B. T., Klunk, W. E., Bacskai, B. J., and Swager, T. M. (2005) In vivo optical imaging of amyloid aggregates in brain: design of fluorescent markers. *Angew. Chem., Int. Ed. 44*, 5452–5456.

(31) Raymond, S. B., Skoch, J., Hills, I. D., Nesterov, E. E., Swager, T. M., and Bacskai, B. J. (2008) Smart optical probes for near-infrared fluorescence imaging of Alzheimer's disease pathology. *Eur. J. Nucl. Med. Mol. Imaging 35* (Suppl 1), S93–S98.

(32) Ran, C., Xu, X., Raymond, S. B., Ferrara, B. J., Neal, K., Bacskai, B. J., Medarova, Z., and Moore, A. (2009) Design, synthesis, and testing of difluoroboron-derivatized curcumins as near-infrared probes for in vivo detection of amyloid-β deposits. *J. Am. Chem. Soc. 131*, 15257–15261.

(33) Ran, C., Zhao, W., Moir, R. D., and Moore, A. (2011) Non-conjugated small molecule FRET for differentiating monomers from higher molecular weight amyloid β species. *PLos One 6*, e19362.

(34) Weissleder, R., and Mahmood, U. (2001) Molecular imaging. *Radiology 219*, 316–333.

(35) Chang, W. M., Dakanali, M., Capule, C. C., Sigurdson, C. J., Yang, J., and Theodorakis, E. A. (2011) ANCA: a family of fluorescent probes that bind and stain amyloid plaques in human tissue. *ACS Chem. Neurosci. 2*, 249–255.

(36) Liu, K., Guo, T. L., Chojnacki, J., Lee, H. G., Wang, X., Siedlak, S. L., Rao, W., Zhu, X., and Zhang, S. (2011) Bivalent ligand containing curcumin and cholesterol as a fluorescence probe for Aβ plaques in Alzheimer's disease, *ACS Chem Neurosci.*, DOI: 10.1021/cn200122j.

(37) Lee, J. S., Kang, N. Y., Kim, Y. K., Samanta, A., Feng, S., Kim, H. K., Vendrell, M., Park, J. H., and Chang, Y. T. (2009) Synthesis of a BODIPY library and its application to the development of live cell glucagon imaging probe. *J. Am. Chem. Soc. 131*, 10077–10082.

(38) Ojida, A., Sakamoto, T., Inoue, M. A., Fujishima, S. H., Lippens, G., and Hamachi, I. (2009) Fluorescent BODIPY-based Zn(II) complex as a molecular probe for selective detection of neurofibrillary tangles in the brains of Alzheimer's disease patients. *J. Am. Chem. Soc. 131*, 6543–6548.

(39) Sun, Z. N., Wang, H. L., Liu, F. Q., Chen, Y., Tam, P. K., and Yang, D. (2009) BODIPY-based fluorescent probe for peroxynitrite detection and imaging in living cells. *Org. Lett. 11*, 1887–1890.

(40) Lee, J. J., Lee, S. C., Zhai, D., Ahn, Y. H., Yeo, H. Y., Tan, Y. L., and Chang, Y. T. (2011) Bodipy-diacrylate imaging probes for targeted proteins inside live cells. *Chem. Commun. (Cambrideg, U.K.) 47*, 4508–4510.

(41) Ono, M., Ishikawa, M., Kimura, H., Hayashi, S., Matsumura, K., Watanabe, H., Shimizu, Y., Cheng, Y., Cui, M., Kawashima, H., and Saji, H. (2010) Development of dual functional SPECT/fluorescent probes for imaging cerebral β-amyloid plaques. *Bioorg. Med. Chem. Lett. 20*, 3885–3888.

(42) Parhi, A. K., Kung, M. P., Ploessl, K., and Kung, H. F. (2008) Synthesis of fluorescent probes based on stilbenes and diphenylacetylenes targeting β-amyloid plaques. *Tetrahedron Lett. 49*, 3395–3399.

(43) Smith, N. W., Alonso, A., Brown, C. M., and Dzyuba, S. V. (2010) Triazole-containing BODIPY dyes as novel fluorescent probes for soluble oligomers of amyloid Aβ1–42 peptide. *Biochem. Biophys. Res. Commun. 391*, 1455–1458.

(44) Ono, M., Kung, M. P., Hou, C., and Kung, H. F. (2002) Benzofuran derivatives as Aβ-aggregate-specific imaging agents for Alzheimer's disease. *Nucl. Med. Biol. 29*, 633–642.

(45) Ono, M., Haratake, M., Mori, H., and Nakayama, M. (2007) Novel chalcones as probes for in vivo imaging of β-amyloid plaques in Alzheimer's brains. *Bioorg. Med. Chem. 15*, 6802–6809.

(46) Ono, M., Yoshida, N., Ishibashi, K., Haratake, M., Arano, Y., Mori, H., and Nakayama, M. (2005) Radioiodinated flavones for in vivo imaging of β-amyloid plaques in the brain. *J. Med. Chem. 48*, 7253–7260.

(47) Sutharsan, J., Dakanali, M., Capule, C. C., Haidekker, M. A., Yang, J., and Theodorakis, E. A. (2010) Rational design of amyloid binding agents based on the molecular rotor motif. *ChemMedChem 5*, 56–60.

(48) Hsiao, K., Chapman, P., Nilsen, S., Eckman, C., Harigaya, Y., Younkin, S., Yang, F., and Cole, G. (1996) Correlative memory deficits, Aβ elevation, and amyloid plaques in transgenic mice. *Science 274*, 99–102.

(49) Ono, M., Cheng, Y., Kimura, H., Cui, M. C., Kagawa, S., Nishii, R., and Saji, H. (2011) Novel ^{18}F-labeled benzofuran derivatives with improved properties for positron emission tomography (PET) imaging of β-amyloid plaques in Alzheimer's brains. *J. Med. Chem. 54*, 2971–2979.

(50) Cheng, Y., Ono, M., Kimura, H., Kagawa, S., Nishii, R., Kawashima, H., and Saji, H. (2010) Fluorinated benzofuran derivatives for PET imaging of β-amyloid plaques in Alzheimer's disease brains. *ACS Med. Chem. Lett. 1*, 321–325.

(51) Cheng, Y., Ono, M., Kimura, H., Kagawa, S., Nishii, R., and Saji, H. (2010) A novel ^{18}F-labeled pyridyl benzofuran derivative for imaging of β-amyloid plaques in Alzheimer's brains. *Bioorg. Med. Chem. Lett. 20*, 6141–6144.

(52) Skovronsky, D. M., Zhang, B., Kung, M. P., Kung, H. F., Trojanowski, J. Q., and Lee, V. M. Y. (2000) In vivo detection of amyloid plaques in a mouse model of Alzheimer's disease. *Proc. Natl. Acad. Sci. U.S.A. 93*, 7609–7614.

(53) Atilgan, S., Ozdemir, T., and Akkaya, E. U. (2008) A sensitive and selective ratiometric near IR fluorescent probe for zinc ions based on the distyryl-bodipy fluorophore. *Org. Lett. 10*, 4065–4067.

(54) Awuah, S. G., Polreis, J., Biradar, V., and You, Y. (2011) Singlet oxygen generation by novel NIR BODIPY dyes. *Org. Lett. 13*, 3884–3887.

(55) Kubo, Y., Watanabe, K., Nishiyabu, R., Hata, R., Murakami, A., Shoda, T., and Ota, H. (2011) Near-infrared absorbing boron-dibenzopyrromethenes that serve as light-harvesting sensitizers for polymeric solar cells. *Org. Lett. 13*, 4574–4577.

J Pharmacol Sci **118**, 338 – 344 (2012)

Journal of Pharmacological Sciences

Forum Minireview

Molecular Approaches to the Treatment, Prophylaxis, and Diagnosis of Alzheimer's Disease: Novel PET/SPECT Imaging Probes for Diagnosis of Alzheimer's Disease

Masahiro Ono[1,*] and Hideo Saji[1]

[1]*Graduate School of Pharmaceutical Sciences, Kyoto University, 46-29 Yoshida Shimoadachi-cho, Sakyo-ku, Kyoto 606-8501, Japan*

Received October 15, 2011; Accepted November 9, 2011

Abstract. Alzheimer's disease (AD) is a neurodegenerative disease of the brain associated with irreversible cognitive decline, memory impairment, and behavioral changes. Postmortem brains of AD patients reveal neuropathologic features, in particular the presence of senile plaques (SPs) and neurofibrillary tangles (NFTs), which contain β-amyloid peptides and highly phosphorylated tau proteins. Currently, AD can only be definitively confirmed by postmortem histopathologic examination of SPs and NFTs in the brain. Therefore, SPs and NFTs in the brain may be useful as biomarkers for the differential diagnosis of AD; the detection of individual SPs and NFTs in vivo by positron-emission tomography (PET) or single-photon emission computed tomography (SPECT) should improve diagnosis and also accelerate discovery of effective therapeutic agents for AD. Many PET/SPECT imaging probes for SPs have already been developed. Several of the PET probes have been shown in clinical trials to be useful for the imaging of β-amyloid plaques in living brain tissue. More recently, the development of PET/SPECT probes for in vivo imaging of NFTs is an active area of study in the field of molecular imaging because the appearance of NFT pathology correlates well with clinical severity of dementia. We will review current research on the development of PET/SPECT imaging probes for in vivo detection of SPs and NFTs and their application to diagnosis and therapy of AD.

Keywords: Alzheimer's disease, senile plaque, neurofibrillary tangle, positron-emission tomography (PET), single-photon emission computed tomography (SPECT)

1. Introduction

Alzheimer's disease (AD) is an age-related, progressive neurodegenerative disorder characterized by irreversible dementia: memory loss, a progressive decline in intellectual ability, language impairment, and personality and behavioral changes that eventually interfere with daily life. AD is characterized by abundant senile plaques (SPs) composed of β-amyloid (Aβ) peptides and by numerous neurofibrillary tangles (NFTs) formed by filaments of highly phosphorylated tau proteins in the brain (1). Today, the clinical diagnosis of AD is primarily based on history and memory testing; these examinations are often insensitive and inaccurate, as the early cognitive and behavioral symptoms of AD are difficult to distinguish from age-related cognitive decline. To facilitate the early diagnosis of this disease, there is an urgent need to discover sensitive non-invasive detection methods for biomarkers of AD pathophysiology. Toward this end, nuclear imaging techniques such as positron-emission tomography (PET) and single-photon emission computed tomography (SPECT) have been employed. Radionuclide-labeled agents targeting the Aβ plaques in the brain may greatly facilitate the early diagnosis of AD, as well as new anti-amyloid and anti-tau therapies (2 – 6). The differential diagnosis for AD includes a large number

*Corresponding author. ono@pharm.kyoto-u.ac.jp
Published online in J-STAGE on March 2, 2012 (in advance)
doi: 10.1254/jphs.11R08FM

of other diseases such as vascular dementia, frontal temporal lobar dementia (FTLD) complex, and dementia with Lewy bodies (DLB), as well as more rare neurodegenerative diseases such as Creutzfeld-Jacob disease (CJD). Here, we review the current status of development of PET/SPECT probes for in vivo imaging of SPs and NFTs in the brain.

2. PET/SPECT imaging probes for SPs

The formation of Aβ plaques in the brain is generally accepted as the initial neurodegenerative event in AD (1, 7). Therefore, several research groups have developed PET/SPECT probes that target Aβ plaques in AD brains. Initial studies with [^{18}F]-2-(1-(2-(*N*-(2-fluoroethyl)-*N*-methylamino)naphthalene-6-yl)ethylidene)malononitrile (FDDNP) (8, 9) (Fig. 1) were the first to demonstrate differential uptake and retention in the brain of AD patients. PET imaging studies in humans suggest that FDDNP exhibits higher retention in regions of the brain suspected of containing either NFTs or Aβ plaques, indicating that it is not selectively measuring Aβ plaques in AD brains. Thereafter, many clinical studies with PET suggested that [^{11}C]4-*N*-methylamino-4′-hydroxystilbene (SB-13) (5, 10), [^{11}C]-2-(4′-(methylaminophenyl)-6-hydroxybenzothiazole (PIB) (11, 12), [^{11}C]2-(2-[2-dimethylaminothiazol-5-yl]ethenyl)-6-(2-[fluoro]ethoxy)benzoxazole (BF-227) (13), and [^{11}C]-2-[6-(methylamino)pyridin-3-yl]-1,3-benzothiazol-6-ol (AZD2184) (14, 15) differed in their uptake and retention in the brain between AD patients and controls (Fig. 1). Among these compounds, PIB is the best characterized PET imaging agent for Aβ plaques in the brain; over the past few years, PIB imaging has been reported in thousands of AD patients. The utility of PIB to image Aβ plaques in the brain has provided considerable impetus for further refinement of this technique. However, since PIB is labeled with ^{11}C, a positron-emitting isotope with a short half-life ($t_{1/2}$: 20 min), the radiosynthesis of [^{11}C]PIB in a relatively short time are needed, and its use is also limited to major academic PET facilities with on-site cyclotrons and sophisticated radiochemistry laboratories. Such practical challenges of using PIB labeled with ^{11}C have limited its potential as a diagnostic tool on a routine basis. Alternative tracers labeled with ^{18}F, which has a longer half-life ($t_{1/2}$: 110 min), may be more useful as PET imaging agents for detection and quantification of Aβ plaques; therefore, recent efforts have focused on the development of comparable agents labeled with ^{18}F. More recently, the PIB analogue 2-(3-[^{18}F]-fluoro-4-methylamino-phenyl)benzothiazol-6-ol (GE-067, flutemetamol) (16 – 18), a stilbene derivative (*E*)-4-(*N*-methylamino)-4′-(2-(2-(2-[^{18}F]-fluoroethoxy)ethoxy)ethoxy)-stilbene (BAY94-9172, florbetaben) (19 – 21), and a styryl pyridine derivative (*E*)-4-(2-(6-(2-(2-(2-([^{18}F]-fluoroethoxy)ethoxy)ethoxy)pyridyn-3-ylvinyl)-*N*-methyl benzenamine (AV-45, florbetapir) (22 – 27) have been demonstrated to be useful for the imaging of Aβ plaques in living brain tissue in phase III clinical trials (Fig. 1) (6).

In the search for PET imaging agents with improved properties, we have recently developed a series of fluorinated benzofuran derivatives for use as potential ^{18}F-labeled tracers in the imaging of Aβ plaques by PET.

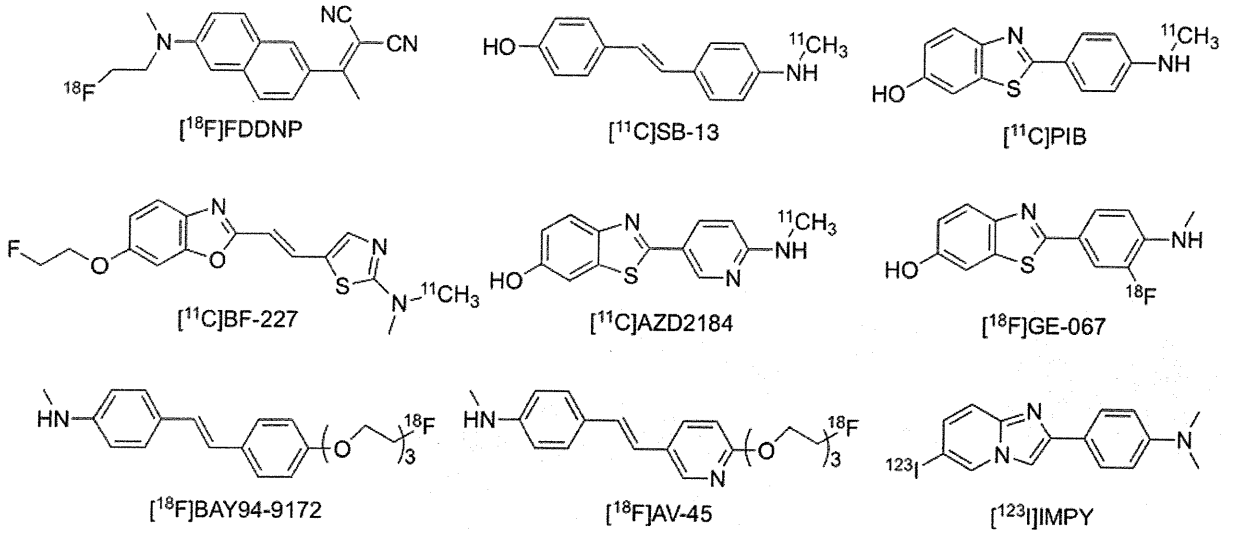

Fig. 1. Chemical structure of PET/SPECT imaging probes for detection of senile plaques.

First, based on our previous research on radioiodinated and ^{11}C-labeled benzofuran derivatives (28, 29), we developed 4-(5-(2-(2-(2-fluoroethoxy)ethoxy)ethoxy) benzofuran-2-yl)-*N,N*-dimethylbenzenamine (FPHBF-1, Fig. 2), which has a fluoropolyethylene glycol side chain and a dimethylamino phenyl group (30). Although the penetration of brain tissues by this tracer was encouraging, the slow washout of this probe from the normal mouse brain made it unsuitable for imaging in vivo. Therefore, it will be critical to fine-tune the kinetics of the uptake and washout of existing benzofuran derivatives. Previous results regarding brain uptake and clearance indicate that high lipophilicity is one of the reasons behind the compound's slow washout kinetics (11, 29, 31, 32).

To further improve the pharmacokinetics of radioactive substances in the brain, we planned to develop a novel, less lipophilic fluorinated pyridyl benzofuran derivative by displacing the phenyl group in phenyl benzofuran with a pyridyl group. Therefore, we designed and synthesized 5-(5-(2-(2-(2-fluoroethoxy)ethoxy)ethoxy) benzofuran-2-yl)-*N*-methylpyridin-2-amine (FPYBF-2, Fig. 2), which has a fluoropolyethylene glycol side chain and a monomethylamino pyridyl group (33). In in vitro experiments, FPYBF-2 displayed high affinity for Aβ(1-42) aggregates (K_i = 2.41 nM). In biodistribution experiments using normal mice, it displayed high uptake in the brain (8.18%ID/g at 2 min postinjection), and the radioactivity washed out of the brain rapidly (3.87%ID/g at 60 min postinjection, respectively); this feature is highly desirable for Aβ imaging agents. To further characterize the compound's potential in living brain tissue, we carried out ex vivo autoradiography in Tg2576 mice, using wild-type mice as age-matched controls (Fig. 3). Autoradiography with [^{18}F]FPYBF-2 showed distinctive labeling of Aβ plaques in the Tg2576 mouse brain (Fig. 3A), whereas wild-type mouse brain showed no such labeling (Fig. 3B). Aβ plaques were confirmed to be present by costaining of sections with thioflavin-S, a dye commonly used to stain Aβ plaques (Fig. 3C). These results suggest that [^{18}F]FPYBF-2 penetrated the blood–brain barrier and selectively labeled Aβ plaques in the brain, as reflected by the biodistribution experiments and in vitro binding assays. Furthermore, the specific labeling of Aβ plaques by [^{18}F]FPYBF-2 was observed in autoradiographs of sections of AD brain obtained from autopsies. These results suggested that [^{18}F]FPYBF-2 is a promising PET probe for imaging cerebral Aβ plaques; the compound is now undergoing preclinical evaluation.

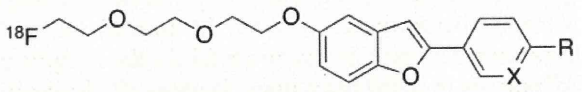

FPYBF-1 (X = N, R = NMe_2)
FPHBF-1 (X = CH, R = NMe_2)
FPYBF-2 (X = N, R = NHMe)
FPHBF-2 (X = CH, R = NHMe)

Fig. 2. Chemical structure of ^{18}F-labeled benzofuran derivatives.

3. PET/SPECT probes for NFTs

While many PET/SPECT probes have been developed for detecting SPs, few compounds for targeting NFTs

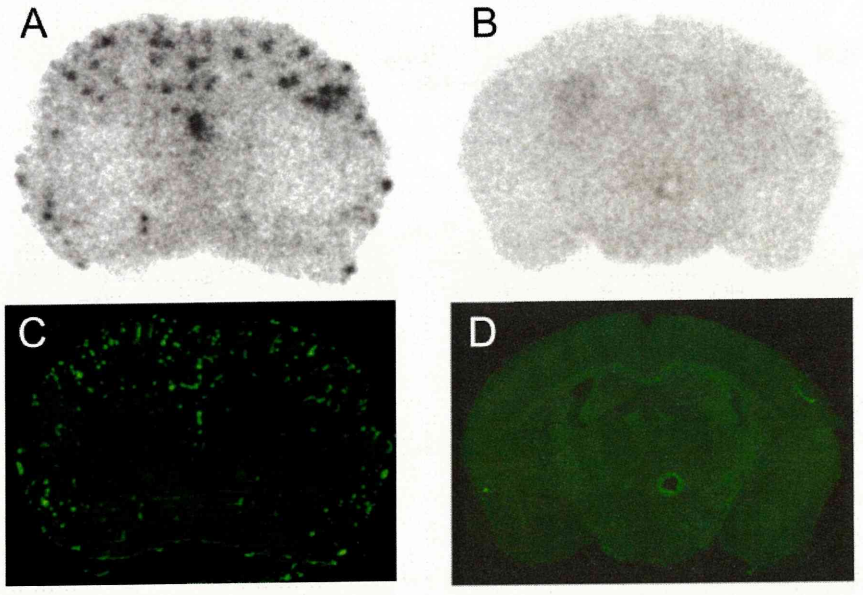

Fig. 3. Ex vivo autoradiography in brain sections from a Tg 2576 mouse (A) and a wild-type mouse (B) using [^{18}F]FPYBF-2. The same sections were also stained with thioflavin-S (C and D). Reproduced from Ref. 33 with permission.

have been reported. Previous neuropathological research suggests that the deposition of NFTs occurs before the manifestation of clinical symptoms in AD. These reports suggest that even in the very early stages of AD, patients display considerable numbers of NFTs in the entorhinal cortex and hippocampus, sufficient for a neuropathological diagnosis. Furthermore, NFT deposition in the entorhinal cortex is closely related with neuronal loss in very early AD patients (34 – 37). Thus, in vivo imaging of NFTs in conjunction with imaging of Aβ plaques would be useful for the early and accurate diagnosis of AD. A quantitative evaluation of tau pathology could also be helpful in tracking the severity of dementia because the molecular pathology correlates well with the clinical severity of dementia.

Several papers have reported that FDDNP (38), FSB (39), and curcumin (40) can bind to not only NFTs but also Aβ plaques in the brain. Okamura and colleagues screened over 2000 small molecules in order to develop novel radiotracers with high affinity and selectivity for tau pathology/NFTs (41). Consequently, they identified a series of novel quinoline and benzimidazole derivatives that bind NFTs such as [^{11}C]BF-158 (Fig. 4). However, these compounds are not completely specific to tau, because they also bind to Aβ plaques. Further study of those compounds led to the design and synthesis of a novel imaging agent, [^{18}F]THK523 (Fig. 4) (42). In vitro binding studies demonstrated that [^{18}F]THK523 binds with higher affinity to a larger number of binding sites on recombinant tau than on Aβ fibrils. Autoradiographic and histofluorescence analyses of human hippocampal serial sections from AD patients exhibited positive THK523 binding that co-localized with immunoreactive tau pathology, but did not highlight Aβ plaques. Micro PET analysis demonstrated significantly higher retention of [^{18}F]THK523 in tau transgenic mice brains compared with their wild-type littermates or APP/PS1 mice. The authors concluded that the preclinical examination of THK523 has demonstrated its high affinity and selectivity for tau pathology both in vitro and in vivo; thus, [^{18}F]THK523 fulfils the criteria for a ligand that could be used in human imaging trials.

More recently, the effects of rhodanine and thiohydantoin derivatives on the formation, extension, and destabilization of tau aggregates have been studied in vitro (43). These derivatives dose-dependently inhibited the formation of tau aggregates and also destabilized preformed tau aggregates, indicating that they could directly bind or interact with the aggregates. In our recent study, we designed and synthesized three novel radioiodinated rhodanine and thiohydantoin (TH) derivatives (Fig. 4) and evaluated their biological activities as SPECT imaging agents targeting NFTs (44). In experiments in vitro using tau and Aβ aggregates, the TH derivative TH2 exhibited highly specific binding to tau aggregates. In hippocampal sections obtained from AD patients, TH2 intensely stained NFTs. In experiments using normal mice, [^{125}I]TH2 exhibited sufficient uptake (1.54%ID/g, 2 min postinjection) into the brain, and rapid washout (0.25%ID/g, 60 min postinjection). These results suggest that [^{123}I]TH2 should be further investigated as a potential imaging agent for detecting tau pathology.

Furthermore, Honson et al. screened a library containing 72,455 compounds to determine the feasibility of distinguishing tau aggregates from Aβ aggregates using small molecules (45, 46). Among the compounds that bound to tau aggregates, a phenyldiazenyl benzothiazole (PDB) derivative 4-[2-(5-methoxy-2-benzothiazolyl) diazenyl]-*N,N*-dimethyl-benzenamine exhibited the highest affinity for tau aggregates, with a two-fold selectivity for tau relative to Aβ aggregates (45). A more recent paper reported that the PDB derivative strongly binds to tau aggregates at sites that at least partially overlap with those bound by thioflavin-S (46). These findings prompted us to use the PDB as a core structure in the development of agents for imaging NFTs. We designed novel radioiodinated PDB derivatives as SPECT imaging agents, substituting a methoxy group with a radioiodine

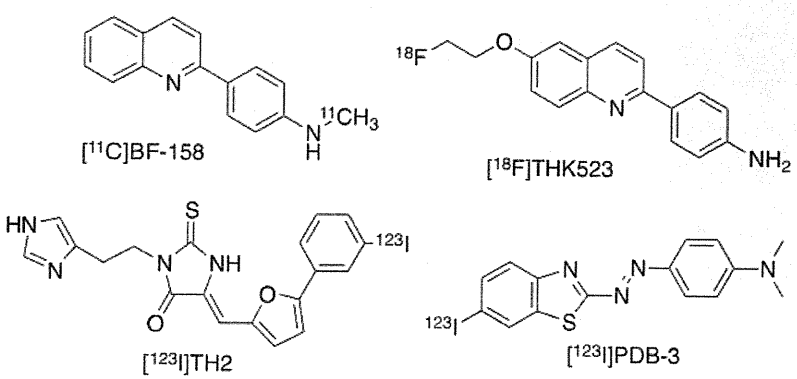

Fig. 4. Chemical structure of PET/SPECT imaging probes for detection of neurofibrillary tangles.

at position 7 and introducing an electron-donating group (dimethylamino, monomethylamino, or amino group) at position 4 of the phenyl group (Fig. 4) (47). In in vitro binding experiments using tau aggregates, the derivatives, especially PDB-3 with the dimethylamino group, exhibited high affinity for tau aggregates. To confirm the affinity of PDB-3 for NFTs in the AD brain, fluorescent staining was carried out in sections of brain tissue (Fig. 5). Numerous fluorescent spots were detected in the entorhinal cortex of AD brain sections (Fig. 5A). The fluorescent labeling pattern corresponded to that obtained with thioflavin-S (Fig. 5B). These results demonstrate the feasibility of using [^{123}I]PDB-3 as a probe for detecting NFTs in the brains of AD patients. In biodistribution experiments using normal mice, the PDB derivatives displayed sufficient brain uptake, but persistent radioactivity in the brain made them unsuitable for imaging NFTs in vivo. Appropriate structural changes to the PDB scaffold may lead to useful NFT imaging agents.

4. Conclusions

As summarized in this review, many promising PET probes for SPs have been developed and tested in clinical studies. Several of these compounds, including GE067, BAY-94-9172, and AV-45, are in active commercial development. On the other hand, no existing PET/SPECT imaging agents allow an evaluation of tau pathology in AD brains, although there are several reports that tau imaging probes are being developed. Therefore, PET/SPECT probes with high specific affinity for NFTs are urgently required. Development of such novel probes will not only contribute to improved early diagnosis of AD, but will also accelerate the discovery of effective therapeutic agents for AD in the near future. Furthermore, Aβ42 and tau in the cerebrospinal fluid (CSF) have recently been accepted as sensitive biomarkers for diagnosis of AD and prediction of onset of AD from mild cognitive impairment [for details, see the article written by M. Shoji in this Forum Minireview series (Ref. 48)]. Combination of PET/SPECT imaging with the detection of Aβ and tau in CSF should enhance diagnostic accuracy of AD.

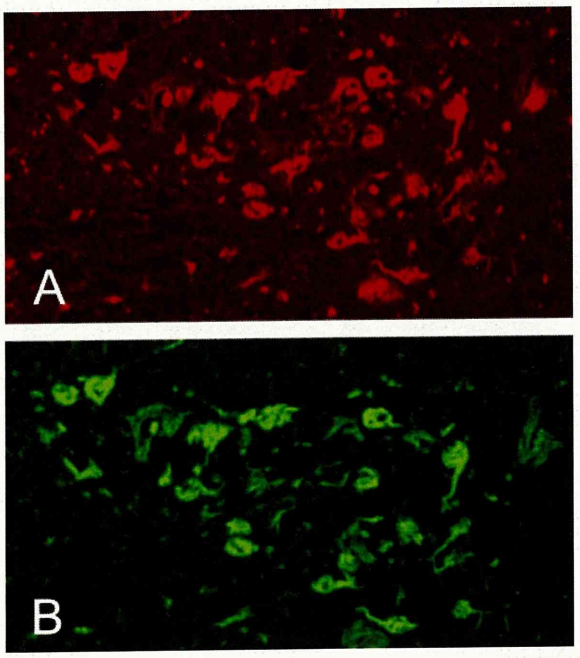

Fig. 5. Fluorescent staining with PDB-3 (A) or thioflavin-S (B) in the entorhinal cortex of a section of AD brain. Reproduced from Ref. 47 with permission.

Acknowledgments

Our research described in this minireview was supported by a Grant-in-Aid for Young Scientists from the Ministry of Education, Culture, Sports, Science, and Technology; the Industrial Technology Research Grant Program from New Energy and Industrial Technology Development Organization (NEDO); the Program for Promotion of Fundamental Biomedical Innovation (NIBIO); a Health Labour Sciences Research Grant; and the Funding Program for Next Generation World-Leading Researchers (NEXT Program).

References

1 Selkoe DJ. Alzheimer's disease: genes, proteins, and therapy. Physiol Rev. 2001;81:741–766.
2 Mathis CA, Wang Y, Klunk WE. Imaging β-amyloid plaques and neurofibrillary tangles in the aging human brain. Curr Pharm Des. 2004;10:1469–1492.
3 Nordberg A. PET imaging of amyloid in Alzheimer's disease. Lancet Neurol. 2004;3:519–527.
4 Ono M. Development of positron-emission tomography/single-photon emission computed tomography imaging probes for *in vivo* detection of β-amyloid plaques in Alzheimer's brains. Chem Pharm Bull (Tokyo). 2009;57:1029–1039.
5 Verhoeff NP, Wilson AA, Takeshita S, Trop L, Hussey D, Singh K, et al. In-vivo imaging of Alzheimer disease β-amyloid with [^{11}C]SB-13 PET. Am J Geriatr Psychiatry. 2004;12:584–595.
6 Kung HF, Choi SR, Qu W, Zhang W, Skovronsky D. ^{18}F stilbenes and styrylpyridines for PET imaging of Aβ plaques in Alzheimer's disease: a miniperspective. J Med Chem. 2010;53:933–941.
7 Hardy JA, Higgins GA. Alzheimer's disease: the amyloid cascade hypothesis. Science. 1992;256:184–185.
8 Agdeppa ED, Kepe V, Liu J, Flores-Torres S, Satyamurthy N, Petric A, et al. Binding characteristics of radiofluorinated 6-dialkylamino-2-naphthylethylidene derivatives as positron emission tomography imaging probes for β-amyloid plaques in Alzheimer's disease. J Neurosci. 2001;21:RC189.
9 Shoghi-Jadid K, Small GW, Agdeppa ED, Kepe V, Ercoli LM, Siddarth P, et al. Localization of neurofibrillary tangles and β-amyloid plaques in the brains of living patients with Alzheimer

disease. Am J Geriatr Psychiatry. 2002;10:24–35.
10 Ono M, Wilson A, Nobrega J, Westaway D, Verhoeff P, Zhuang ZP, et al. ^{11}C-labeled stilbene derivatives as Aβ-aggregate-specific PET imaging agents for Alzheimer's disease. Nucl Med Biol. 2003;30:565–571.
11 Mathis CA, Wang Y, Holt DP, Huang GF, Debnath ML, Klunk WE. Synthesis and evaluation of ^{11}C-labeled 6-substituted 2-arylbenzothiazoles as amyloid imaging agents. J Med Chem. 2003;46:2740–2754.
12 Klunk WE, Engler H, Nordberg A, Wang Y, Blomqvist G, Holt DP, et al. Imaging brain amyloid in Alzheimer's disease with Pittsburgh Compound-B. Ann Neurol. 2004;55:306–319.
13 Kudo Y, Okamura N, Furumoto S, Tashiro M, Furukawa K, Maruyama M, et al. 2-(2-[2-Dimethylaminothiazol-5-yl]ethenyl)-6-(2-[fluoro]ethoxy)benzoxazole: a novel PET agent for in vivo detection of dense amyloid plaques in Alzheimer's disease patients. J Nucl Med. 2007;48:553–561.
14 Johnson AE, Jeppsson F, Sandell J, Wensbo D, Neelissen JA, Jureus A, et al. AZD2184: a radioligand for sensitive detection of β-amyloid deposits. J Neurochem. 2009;108:1177–1186.
15 Swahn BM, Wensbo D, Sandell J, Sohn D, Slivo C, Pyring D, et al. Synthesis and evaluation of 2-pyridylbenzothiazole, 2-pyridylbenzoxazole and 2-pyridylbenzofuran derivatives as ^{11}C-PET imaging agents for β-amyloid plaques. Bioorg Med Chem Lett. 2010;20:1976–1980.
16 Koole M, Lewis DM, Buckley C, Nelissen N, Vandenbulcke M, Brooks DJ, et al. Whole-body biodistribution and radiation dosimetry of ^{18}F-GE067: a radioligand for in vivo brain amyloid imaging. J Nucl Med. 2009;50:818–822.
17 Vandenberghe R, Van Laere K, Ivanoiu A, Salmon E, Bastin C, Triau E, et al. ^{18}F-flutemetamol amyloid imaging in Alzheimer disease and mild cognitive impairment: a phase 2 trial. Ann Neurol. 2010;68:319–329.
18 Nelissen N, Van Laere K, Thurfjell L, Owenius R, Vandenbulcke M, Koole M, et al. Phase 1 study of the Pittsburgh compound B derivative ^{18}F-flutemetamol in healthy volunteers and patients with probable Alzheimer disease. J Nucl Med. 2009;50:1251–1259.
19 Zhang W, Oya S, Kung MP, Hou C, Maier DL, Kung HF. F-18 polyethyleneglycol stilbenes as PET imaging agents targeting Aβ aggregates in the brain. Nucl Med Biol. 2005;32:799–809.
20 Rowe CC, Ackerman U, Browne W, Mulligan R, Pike KL, O'Keefe G, et al. Imaging of amyloid beta in Alzheimer's disease with ^{18}F-BAY94-9172, a novel PET tracer: proof of mechanism. Lancet Neurol. 2008;7:129–135.
21 O'Keefe GJ, Saunder TH, Ng S, Ackerman U, Tochon-Danguy HJ, Chan JG, et al. Radiation dosimetry of β-amyloid tracers ^{11}C-PiB and ^{18}F-BAY94-9172. J Nucl Med. 2009;50:309–315.
22 Zhang W, Kung MP, Oya S, Hou C, Kung HF. ^{18}F-labeled styrylpyridines as PET agents for amyloid plaque imaging. Nucl Med Biol. 2007;34:89–97.
23 Choi SR, Golding G, Zhuang Z, Zhang W, Lim N, Hefti F, et al. Preclinical properties of ^{18}F-AV-45: a PET agent for Aβ plaques in the brain. J Nucl Med. 2009;50:1887–1894.
24 Wong DF, Rosenberg PB, Zhou Y, Kumar A, Raymont V, Ravert HT, et al. *In vivo* imaging of amyloid deposition in Alzheimer disease using the radioligand ^{18}F-AV-45 (flobetapir F 18). J Nucl Med. 2010;51:913–920.
25 Liu Y, Zhu L, Plössl K, Choi SR, Qiao H, Sun X, et al. Optimization of automated radiosynthesis of [^{18}F]AV-45: a new PET imaging agent for Alzheimer's disease. Nucl Med Biol. 2010;37:917–925.
26 Lin KJ, Hsu WC, Hsiao IT, Wey SP, Jin LW, Skovronsky D, et al. Whole-body biodistribution and brain PET imaging with [^{18}F]AV-45, a novel amyloid imaging agent -- a pilot study. Nucl Med Biol. 2010;37:497–508.
27 Clark CM, Schneider JA, Bedell BJ, Beach TG, Bilker WB, Mintun MA, et al. Use of florbetapir-PET for imaging β-amyloid pathology. JAMA. 2010;305:275–283.
28 Ono M, Kung MP, Hou C, Kung HF. Benzofuran derivatives as Aβ-aggregate-specific imaging agents for Alzheimer's disease. Nucl Med Biol. 2002;29:633–642.
29 Ono M, Kawashima H, Nonaka A, Kawai T, Haratake M, Mori H, et al. Novel benzofuran derivatives for PET imaging of β-amyloid plaques in Alzheimer's disease brains. J Med Chem. 2006;49:2725–2730.
30 Cheng Y, Ono M, Kimura H, Kagawa S, Nishii R, Kawashima H, et al. Fluorinated benzofuran derivatives for PET imaging of β-amyloid plaques in Alzheimer's disease brains. ACS Med Chem Lett. 2010;1:321–325.
31 Ono M, Yoshida N, Ishibashi K, Haratake M, Arano Y, Mori H, et al. Radioiodinated flavones for *in vivo* imaging of β-amyloid plaques in the brain. J Med Chem. 2005;48:7253–7260.
32 Ono M, Haratake M, Mori H, Nakayama M. Novel chalcones as probes for *in vivo* imaging of β-amyloid plaques in Alzheimer's brains. Bioorg Med Chem. 2007;15:6802–6809.
33 Ono M, Cheng Y, Kimura H, Cui MC, Kagawa S, Nishii R, et al. Novel ^{18}F-labeled benzofuran derivatives with improved properties for positron emission tomography (PET) imaging of β-amyloid plaques in Alzheimer's brains. J Med Chem. 2011;54:2971–2979.
34 Arriagada PV, Growdon JH, Hedley-Whyte ET, Hyman BT. Neurofibrillary tangles but not senile plaques parallel duration and severity of Alzheimer's disease. Neurology. 1992;42:631–639.
35 Braak H, Braak E. Entorhinal-hippocampal interaction in mnestic disorders. Hippocampus. 1993;3:239–246.
36 Gomez-Isla T, Hollister R, West H, Mui S, Growdon JH, Petersen RC, et al. Neuronal loss correlates with but exceeds neurofibrillary tangles in Alzheimer's disease. Ann Neurol. 1997;41:17–24.
37 Gomez-Isla T, Wasco W, Pettingell WP, Gurubhagavatula S, Schmidt SD, Jondro PD, et al. A novel presenilin-1 mutation: increased β-amyloid and neurofibrillary changes. Ann Neurol. 1997;41:809–813.
38 Small GW, Kepe V, Ercoli LM, Siddarth P, Bookheimer SY, Miller KJ, et al. PET of brain amyloid and tau in mild cognitive impairment. N Engl J Med. 2006;355:2652–2663.
39 Velasco A, Fraser G, Delobel P, Ghetti B, Lavenir I, Goedert M. Detection of filamentous tau inclusions by the fluorescent Congo red derivative FSB [(trans,trans)-1-fluoro-2,5-bis(3-hydroxycarbonyl-4-hydroxy)styrylbenzene]. FEBS Lett. 2008;582:901–906.
40 Mohorko N, Repovs G, Popovic M, Kovacs GG, Bresjanac M. Curcumin labeling of neuronal fibrillar tau inclusions in human brain samples. J Neuropathol Exp Neurol. 2010;69:405–414.
41 Okamura N, Suemoto T, Furumoto S, Suzuki M, Shimadzu H, Akatsu H, et al. Quinoline and benzimidazole derivatives: candidate probes for *in vivo* imaging of tau pathology in Alzheimer's disease. J Neurosci. 2005;25:10857–10862.

42 Fodero-Tavoletti MT, Okamura N, Furumoto S, Mulligan RS, Connor AR, McLean CA, et al. ^{18}F-THK523: a novel *in vivo* tau imaging ligand for Alzheimer's disease. Brain. 2011;134: 1089–1100.
43 Bulic B, Pickhardt M, Khlistunova I, Biernat J, Mandelkow EM, Mandelkow E, et al. Rhodanine-based tau aggregation inhibitors in cell models of tauopathy. Angew Chem Int Ed Engl. 2007; 46:9215–9219.
44 Ono M, Hayashi S, Matsumura K, Kimura H, Okamoto Y, Ihara M, et al. Rhodanine and thiohydantoin derivatives for detecting tau pathology in Alzheimer's brains. ACS Chem Neurosci. 2011;2:269–275.
45 Honson NS, Johnson RL, Huang W, Inglese J, Austin CP, Kuret J. Differentiating Alzheimer disease-associated aggregates with small molecules. Neurobiol Dis. 2007;28:251–260.
46 Honson NS, Jensen JR, Abraha A, Hall GF, Kuret J. Small-molecule mediated neuroprotection in an *in situ* model of tauopathy. Neurotox Res. 2009;15:274–283.
47 Matsumura K, Ono M, Hayashi S, Kimura H, Okamoto Y, Ihara M, et al. Phenyldiazenyl benzothiazole derivatives as probes for *in vivo* imaging of neurofibrillary tangles in Alzheimer's disease brains. Med Chem Comm. 2011;2:596–600.
48 Shoji M. Molecular approaches to the treatment, prophylaxis, and diagnosis of Alzheimer's disease: Clinical molecular and genetic studies on Alzheimer's disease. J Pharmacol Sci. 2012; 118:345–349.

Journal of Medicinal Chemistry

Article

pubs.acs.org/jmc

Technetium-99m Labeled Pyridyl Benzofuran Derivatives as Single Photon Emission Computed Tomography Imaging Probes for β-Amyloid Plaques in Alzheimer's Brains

Yan Cheng,[†] Masahiro Ono,*[,†] Hiroyuki Kimura,[†] Masashi Ueda,[†] and Hideo Saji[†]

[†]Graduate School of Pharmaceutical Sciences, Kyoto University, 46-29 Yoshida Shimoadachi-cho, Sakyo-ku, Kyoto 606-8501, Japan

ABSTRACT: Three novel ^{99m}Tc-labeled pyridyl benzofuran derivatives were tested as potential probes for imaging β-amyloid plaques using single photon emission computed tomography (SPECT). The ^{99m}Tc and corresponding rhenium complexes were synthesized with bis(aminoethanethiol) (BAT) as a chelating ligand. All Re complexes showed affinity for Aβ(1−42) aggregates (K_i = 13.6−149.6 nM). Biodistribution experiments in normal mice revealed that the ^{99m}Tc-labeled derivatives displayed sufficient uptake in the brain (1.41−1.80% ID/g at 2 min postinjection). Notably, [^{99m}Tc]BAT-Bp-2 showed a good initial uptake (1.80% ID/g at 2 min) and a reasonable washout from the brain (0.79% ID/g at 60 min). Ex vivo autoradiography with [^{99m}Tc]BAT-Bp-2 revealed substantial labeling of β-amyloid plaques in sections of brain tissue from Tg2576 transgenic mice but not in the age-matched controls. [^{99m}Tc]BAT-Bp-2 may be a potential SPECT probe for imaging β-amyloid plaques in Alzheimer's brains.

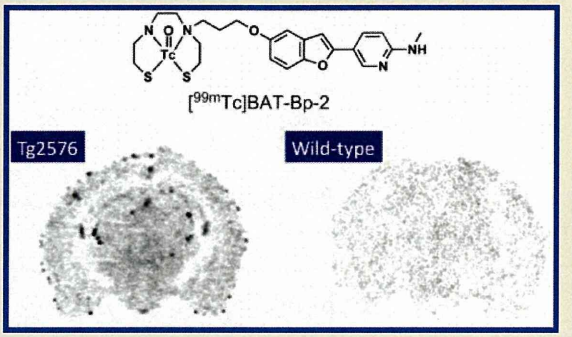

■ INTRODUCTION

Alzheimer's disease (AD) is an age-related brain disorder with the symptoms of memory loss and dementia. Senile plaques (SPs) and neurofibrillary tangles (NFTs), which were first identified in the post-mortem brain of a demented patient by Alois Alzheimer in 1907, have been regarded as the most defining hallmarks of AD.[1] SPs consist of β-amyloid peptides (Aβ) that aggregate into fibrillar, β-pleated sheet structures.[1−3] As β-amyloid plaques deposit years before the onset of AD, their detection in vivo may facilitate the diagnosis of β-amyloidosis in the brain, improve monitoring of the progression of AD, and increase the effectiveness of antiamyloid therapies currently under intense development throughout the world.[1,3]

Over the past several years, remarkable progress in the imaging of β-amyloid plaques in vivo with noninvasive techniques such as positron emission tomography (PET) has brought promise to the early clinical diagnosis of AD. On the basis of the structure of the amyloid-staining agent Thioflavin T or Congo red, several PET imaging probes have been designed and evaluated for imaging β-amyloid plaques such as [^{11}C]4-*N*-methylamino-4′-hydroxystilbene (SB-13),[4,5] [^{11}C]2-(4′-(methylaminophenyl)-6-hydroxybenzothiazole (PIB),[6,7] (2-(3-[^{18}F]-fluoro-4-methyamino-phenyl)benzothiazol-6-ol (GE-067, flutemetamol),[8] (*E*)-4-(*N*-methylamino)-4′-(2-(2-(2-[^{18}F]-fluoroethoxy)ethoxy)ethoxy)-stilbene (BAY94−9172, florbetaben),[9,10] and (*E*)-4-(2-(6-(2-(2-(2-([^{18}F]-fluoroethoxy)-ethoxy)ethoxy)pyridyn-3-ylvinyl)-*N*-methyl benzenamine (AV-45, florbetapir).[10,11] Although these preliminary studies showed promising results, routine clinical use might be hampered by the compounds' short half-lives, high costs, and limited applicability (radioactive nuclide production from a cyclotron, PET camera). More suitable Aβ imaging probes are needed for potential clinical use.

Among medical radioisotopes, ^{99m}Tc ($T_{1/2}$ = 6.01 h, 141 keV) has been most commonly used in diagnostic imaging by single photon emission computed tomography (SPECT) for several reasons: it is readily produced by a ^{99}Mo/^{99m}Tc generator and its physical half-life is compatible with the biological localization and residence time required for imaging. Thus, the development of ^{99m}Tc-labeled Aβ imaging probes will provide simple, convenient, and cost-effective methods for the detection of cerebral β-amyloid plaques in potentially pre-AD conditions such as in cognitively normal elderly subjects and in mild cognitive impairment (MCI) subjects long before the diagnosis of AD.

Initially, ^{99m}Tc-labeled Congo red and chrysamine G derivatives were evaluated as potential Aβ imaging probes, but these large, charged molecules failed to penetrate the blood−brain barrier (BBB).[12,13] Smaller, neutral ^{99m}Tc-labeled ligands have since been reported, such as derivatives of biphenyl,[14] benzothiazle aniline (BTA),[15] chalcone,[16] flavone, aurone,[17] and curcumin[18] (Figure 1), but none of them showed specific binding to β-amyloid plaques in vivo due to either low affinity or low uptake in the brain.

Previously, we designed a series of ^{18}F-labeled benzofuran derivatives and evaluated their biological potential for imaging β-amyloid plaques in AD.[19−21] One of the pyridyl benzofuran derivatives, [^{18}F]FPYBF-2, showed selective affinity for Aβ and good pharmacokinetics in the brain (Figure 2). On the basis of

Received: November 8, 2011
Published: February 24, 2012

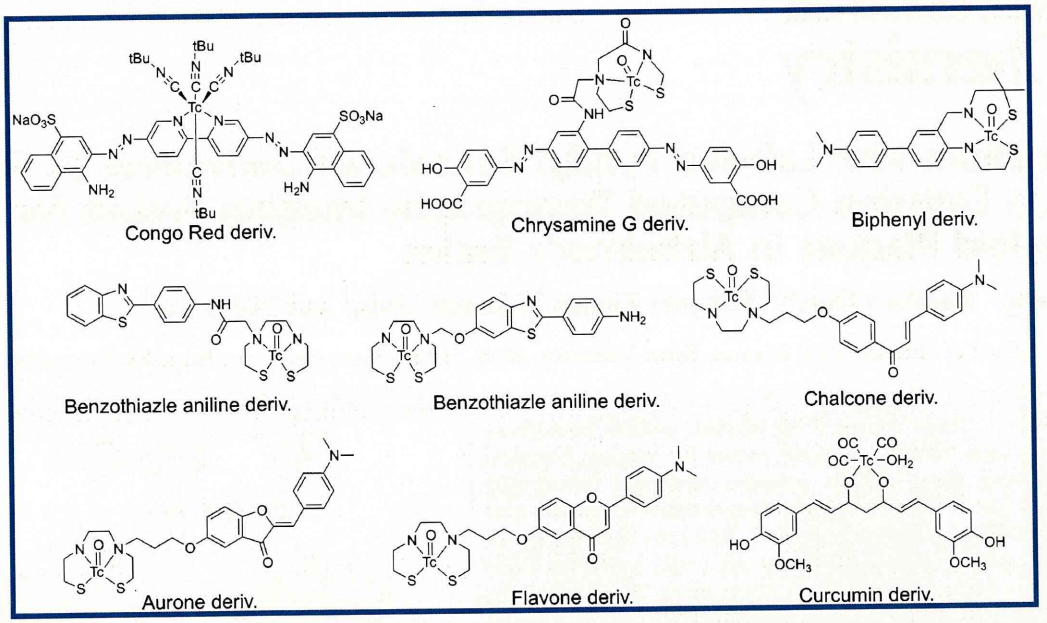

Figure 1. Chemical structure of ^{99m}Tc-labeled Aβ imaging probes reported previously.

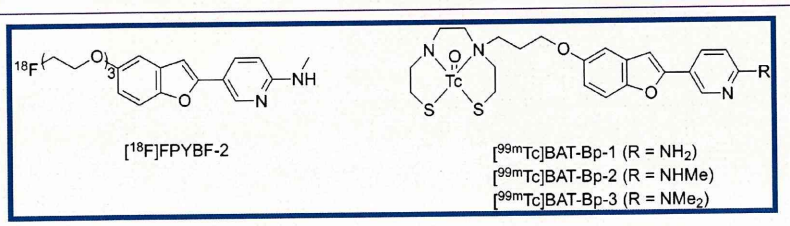

Figure 2. Chemical structure of [^{18}F]FPYBF-2 and ^{99m}Tc-labeled pyridyl benzofuran derivatives reported in the present study.

this encouraging result, we attempted to design novel ^{99m}Tc-labeled Aβ imaging probes with the backbone of pyridyl benzofuran. Different from ^{18}F, a chelating structure is necessary for the transition of metal ^{99m}Tc to an organic molecule. In consideration of the permeability of the BBB, we chose bis(aminoethanethiol) (BAT) as a compact chelating ligand to form a neutral complex with ^{99m}Tc (Figure 2).[16,17,22]

The aim of this study was to synthesize ^{99m}Tc/Re complexes based on pyridyl benzofuran with BAT as the chelating ligand and to study their binding to Aβ and pharmacokinetics in the brain. Herein we report the synthesis and biological evaluation of these novel ^{99m}Tc-labeled pyridyl benzofuran derivatives as potential SPECT agents for imaging β-amyloid plaques in AD.

■ RESULTS AND DISCUSSION

The synthesis of the ^{99m}Tc/Re pyridyl benzofuran derivatives is outlined in Schemes 1, 2, and 3. The key step in the formation of the pyridyl benzofuran backbone was accomplished by Suzuki coupling between 5-methoxybenzofuran-2-boronic acid and 2-amino-5-iodopyridine.[23] Suzuki coupling afforded the desired compound **1** in a yield of 52.1%. Conversion of **1** to the corresponding monomethylamino derivative **3** was achieved by monomethylation with paraformaldehyde and NaOMe (yield 92.1%).[24] Conversion of **1** to the corresponding dimethylamino derivative **9** was achieved by dimethylation with paraformaldehyde and sodium cyanoborohydride (yield 62.0%).[25] A methoxy group of **1**, **3**, and **9** was converted to a hydroxyl group using BBr_3/CH_2Cl_2, which afforded **2**, **4**, and **10** in yields of 98.0%, 99.0%, and 98.9%, respectively.[24] The thiol-protected chelation ligand (TRT-Boc-BAT) was synthesized according to methods reported previously.[16] TRT-Boc-BAT-Br was then synthesized by reacting TRT-Boc-BAT with 1,3-dibromopropane (yield 53.0%). A BAT group was introduced into **2** or **4** by reacting them with TRT-Boc-BAT-Br (**5**, yield 75.2%; **7**, yield 70.3%). A trimethylene group was introduced into **10** as a linker by reacting it with 1,3-dibromopropane (**11**, yield 73.2%) and the chelating ligand BAT was then conjugated with **11** (**12**, yield 45.0%).[16,17] As there is no stable technetium isotope, rhenium, the congener of technetium, has been widely used as a nonradioactive surrogate for the structural identification of technetium complexes.[14,16,17,26,27] Then, we tried to prepare the Re complexes. After deprotection of the thiol groups in **5**, **7**, or **12** in TFA and triethylsilane, the Re complex (**6**, **8**, or **13**) was prepared through a reaction with $(PPh_3)_2ReOCl_3$.

The corresponding ^{99m}Tc complex, **6′** ([^{99m}Tc]BAT-Bp-1), **8′** ([^{99m}Tc]BAT-Bp-2), or **13′** ([^{99m}Tc]BAT-Bp-3), was prepared by a ligand exchange reaction employing the precursor **5**, **7**, or **12** and ^{99m}Tc-glucoheptonate (GH) (Scheme 3).[16,17] The resulting mixture was analyzed by reversed-phase HPLC, showing that a single radioactive complex formed with radiochemical purity higher than 99% after purification by HPLC. The radiochemical identity of the ^{99m}Tc complex was verified by comparative HPLC by using the corresponding Re complex as a reference. The retention times for **6′** ([^{99m}Tc]-BAT-Bp-1), **8′** ([^{99m}Tc]BAT-Bp-2), and **13′** ([^{99m}Tc]BAT-Bp-3) on HPLC (radioactivity) were 9.1, 20.9, and 29.0 min,

Scheme 1[a]

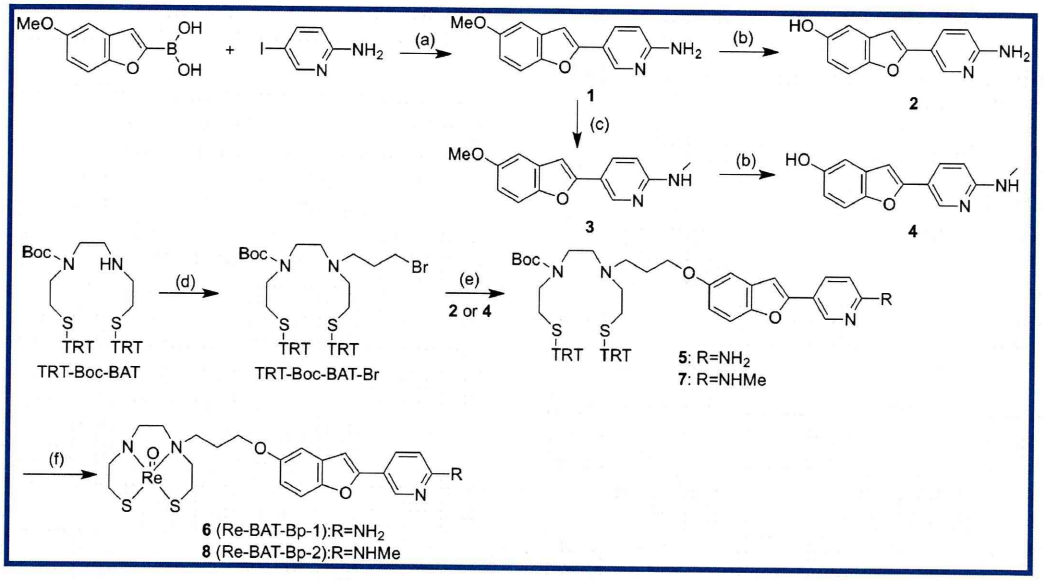

[a]Reagents and conditions: (a) $Pd(Ph_3P)_4$, 2 M Na_2CO_3 (aq)/dioxane; (b) BBr_3, CH_2Cl_2; (c) (1) NaOMe, MeOH, $(CHO)_n$, (2) $NaBH_4$; (d) $Br(CH_2)_3Br$, CH_3CN, K_2CO_3; (e) Cs_2CO_3, acetone, reflux; (f) (1) TFA, Et_3SiH, (2) $(Ph_3P)_2ReOCl_3$, AcONa, CH_2Cl_2/MeOH.

Scheme 2[a]

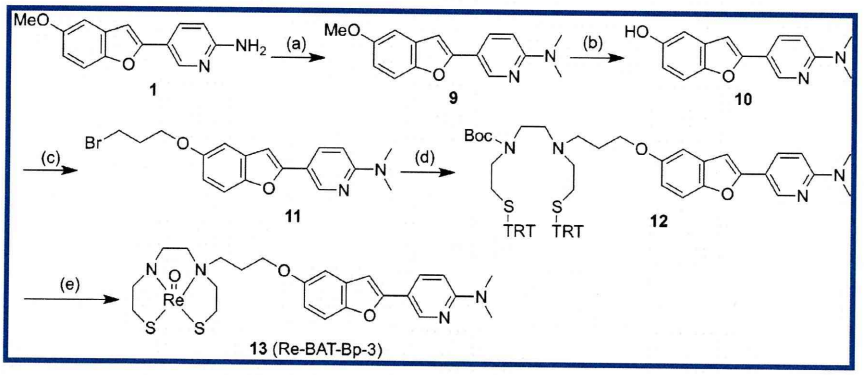

[a]Reagents and conditions: (a) $(CHO)_n$, $NaBH_3CN$, AcOH; (b) BBr_3, CH_2Cl_2; (c) $Br(CH_2)_3Br$, CH_3CN, K_2CO_3; (d) TRT-Boc-BAT, CH_3CN, DIPEA; (e) (1) TFA, Et_3SiH, (2) $(Ph_3P)_2ReOCl_3$, AcONa, CH_2Cl_2/MeOH.

Scheme 3[a]

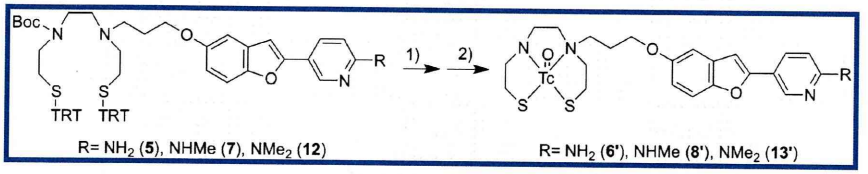

[a]Reagents and conditions: (1) TFA, Et_3SiH; (2) CH_3CN, 0.1 N HCl, ^{99m}Tc-glucoheptonate.

respectively. The retention times of the corresponding Re complexes on HPLC (UV detection) were 8.2, 19.4, and 28.1 min, respectively. The proximate retention times between ^{99m}Tc-labeled tracers and the corresponding Re complexes suggest that the desired ^{99m}Tc-labeled pyridyl benzofuran derivatives were successfully synthesized. Two stereoisomers are known to be generated in ^{99m}Tc complexation reactions of *N*-alkylated BAT complexes.[12,28−30] Although we have not carried out structural analyses by X-ray crystallography of the corresponding rhenium complexes in this study, we presume the major product to be a *syn* isomer because: (1) a single peak of radioactivity was observed in the reaction mixture after ^{99m}Tc-labeling, and (2) most known examples of ^{99m}Tc/Re complexes of this type are predominantly produced as a *syn* isomer.[12,30]

Binding affinity for Aβ aggregates was evaluated with rhenium complexes **6** (Re-BAT-Bp-1), **8** (Re-BAT-Bp-2), and **13** (Re-BAT-Bp-3) according to conventional methods using [^{125}I] 6-iodo-2-(4′-dimethylamino)phenyl-imidazo[1,2-*a*]-pyridine (IMPY).[31,32] Compounds **6**, **8**, and **13** all inhibited the binding of [^{125}I]IMPY in a dose-dependent manner, with

dx.doi.org/10.1021/jm201513c | J. Med. Chem. 2012, 55, 2279−2286

K_i values of 149.6, 32.8, and 13.6 nM, respectively (Table 1). The affinity for Aβ aggregates increased in the order of **13** > **8** > **6**.

Table 1. Inhibition Constants for the Binding of [^{125}I]IMPY to Aβ(1−42) Aggregates

compd	K_i (nM)[a]
Re-BAT-Bp-1 (**6**)	149.6 ± 34.4
Re-BAT-Bp-2 (**8**)	32.8 ± 5.80
Re-BAT-Bp-3 (**13**)	13.6 ± 1.60
IMPY[b]	10.5 ± 1.05
PIB[b]	9.00 ± 1.31

[a]Values are the means ± standard errors of the mean of three independent determinations. [b]Data from ref 21.

The result of the binding study was consistent with that of previous reports,[33−36] indicating that the affinity increased in the order of the *N*,*N*-dimethylated derivative > *N*-monometh ylated derivative > primary amino derivative. The binding affinity of the *N*,*N*-dimethylated derivative (**13**) and *N*-monometh ylated derivative (**8**) was close to that of PIB or IMPY, indicating that they possess sufficient affinity for the imaging of Aβ(1−42) aggregates in vivo. However, the K_i values of these Re complexes were higher than those of fluorinated benzofuran derivatives reported previously.[19−21,24,32] This result suggests that the introduction of the bulky BAT into the pyridyl benzofuran backbone interferes with the binding to Aβ(1−42) aggregates.

To evaluate the pharmacokinetics of ^{99m}Tc-labeled pyridyl benzofuran complexes in the brain, biodistribution experiments were performed in normal mice (Table 2). A biodistribution study provides critical information on penetration of the BBB. Previous papers reported that the optimal measured log *P* value of compounds ranged from 0.1 to 3.5.[1,37] The log *P* values for **6′** ([^{99m}Tc]BAT-Bp-1), **8′** ([^{99m}Tc]BAT-Bp-2), and **13′** ([^{99m}Tc]BAT-Bp-3) were 0.68, 1.35, and 2.09, respectively, indicating that these complexes should penetrate the BBB. As expected, the three ^{99m}Tc-labeled complexes showed uptake into the brain within 10 min ([^{99m}Tc]BAT-Bp-1 and [^{99m}Tc]-BAT-Bp-2 peaked at 2 min postinjection while [^{99m}Tc]BAT-Bp-3 peaked at 10 min), and the radioactivity of all complexes in the brain cleared with time. Among the three, [^{99m}Tc]BAT-Bp-2 showed the highest initial uptake at 2 min postinjection (1.80% ID/g). Although the value was much lower than that of [^{11}C]PIB (7.0% ID/g),[7] [^{18}F]AV-45 (7.33% ID/g),[10,11] or [^{123}I]IMPY (2.88% ID/g),[38] which are currently under clinical trials, it was superior to that of any other ^{99m}Tc-labeled tracer for Aβ imaging reported previously (0.2−1.48% ID/g).[12−18,26]

Table 2. Biodistribution of Radioactivity after Injection of [^{99m}Tc]Tracers in Normal Mice[a]

organ	2 min	10 min	30 min	60 min
		[^{99m}Tc]BAT-Bp-1		
brain	1.59 (0.21)	1.02 (0.03)	0.89 (0.07)	0.97 (0.13)
blood	5.59 (0.53)	2.52 (0.15)	1.83 (0.18)	1.62 (0.24)
liver	15.98 (2.98)	26.01 (3.20)	24.16 (3.56)	22.58 (4.16)
kidney	13.24 (1.17)	13.03 (1.11)	7.96 (1.15)	5.56 (0.87)
pancreas	5.59 (0.58)	5.20 (0.24)	2.83 (0.37)	1.93 (0.29)
spleen	3.54 (0.32)	2.90 (0.16)	1.99 (0.27)	1.51 (0.23)
stomach[b]	1.52 (0.16)	2.89 (0.31)	5.02 (0.46)	5.38 (1.02)
intestine[b]	5.72 (0.57)	12.44 (0.72)	28.94 (2.00)	41.59 (4.31)
lung	11.89 (2.81)	5.33 (0.83)	3.19 (0.36)	2.84 (0.64)
heart	9.83 (1.66)	3.41 (0.16)	1.88 (0.31)	1.35 (0.20)
		[^{99m}Tc]BAT-Bp-2		
brain	1.80 (0.16)	1.30 (0.07)	0.99 (0.09)	0.79 (0.04)
blood	6.01 (0.47)	3.09 (0.13)	2.10 (0.22)	1.60 (0.30)
liver	19.14 (3.78)	30.57 (2.22)	31.29 (2.24)	27.08 (1.11)
kidney	13.96 (1.10)	12.55 (0.72)	8.20 (0.57)	5.62 (0.63)
pancreas	4.36 (0.49)	4.54 (0.13)	2.69 (0.26)	1.55 (0.28)
spleen	3.93 (0.51)	3.80 (0.23)	2.44 (0.23)	1.78 (0.32)
stomach[b]	1.50 (0.24)	3.68 (1.05)	6.06 (0.72)	7.86 (2.14)
intestine[b]	5.60 (0.38)	10.53 (1.02)	23.91 (2.98)	33.24 (2.61)
lung	12.23 (0.94)	6.01 (0.73)	3.98 (0.40)	3.14 (0.61)
heart	13.94 (1.41)	4.12 (0.28)	2.23 (0.37)	1.42 (0.18)
		[^{99m}Tc]BAT-Bp-3		
brain	1.41 (0.17)	1.64 (0.27)	1.08 (0.12)	0.79 (0.07)
blood	8.11 (2.00)	3.90 (0.41)	3.50 (0.80)	1.69 (0.21)
liver	33.85 (4.81)	38.71 (4.35)	37.30 (2.61)	34.75 (5.47)
kidney	19.32 (1.13)	14.61 (1.93)	11.62 (0.93)	6.74 (0.69)
pancreas	6.61 (1.02)	7.16 (0.66)	4.04 (0.70)	3.18 (1.90)
spleen	6.53 (1.70)	5.82 (0.64)	4.15 (0.76)	2.48 (0.32)
stomach[b]	2.78 (0.45)	6.13 (1.22)	11.62 (1.79)	11.90 (2.51)
intestine[b]	6.79 (0.31)	14.70 (4.01)	34.88 (1.83)	45.93 (5.12)
lung	19.17 (2.93)	9.98 (3.06)	6.97 (0.78)	3.87 (0.34)
heart	19.24 (2.77)	7.43 (0.93)	4.03 (0.51)	1.99 (0.18)

[a]Expressed as % injected dose per gram. Each value represents the mean (SD) for five animals at each interval. [b]Expressed as % injected dose per organ.

The $brain_{2min}/brain_{60min}$ ratio is generally used as an index for evaluating radioactivity pharmacokinetics in vivo. The $brain_{2min}/brain_{60min}$ ratio of [^{99m}Tc]BAT-Bp-1, [^{99m}Tc]BAT-Bp-2, and [^{99m}Tc]BAT-Bp-3 was 1.64, 2.28, and 1.78, respectively, indicating that [^{99m}Tc]BAT-Bp-2 provided the best profile of radioactivity in the brain among not only the three ligands tested here but also all ^{99m}Tc ligands reported previously.[13−17,26] Although the $brain_{2min}/brain_{60min}$ ratio of [^{99m}Tc]BAT-Bp-2 was lower than that of [^{11}C]PIB (11.7),[6] [^{18}F]AV-45 (3.89),[11] and [^{123}I]IMPY (14.4),[38] it was similar to that of [^{18}F]FPYBF-2 (2.32), which was previously reported as a ^{18}F-labeled pyridyl benzofuran derivative.[21] On the basis of the results of binding affinity in vitro and biodistribution in normal mice, [^{99m}Tc]BAT-Bp-2 was further evaluated for binding to β-amyloid plaques in Tg2576 transgenic mice.

Next, ex vivo autoradiography was carried out using Tg2576 transgenic mice (27-month-old) and wild-type mice (27-month-old) as age-matched controls (Figure 3). Tg2576 transgenic mice have been widely used for in vitro and in vivo evaluations of Aβ imaging agents because of marked Aβ deposition in the brain.[39] The brain was removed at 30 min postinjection for autoradiography. Autoradiographic images revealed extensive labeling of β-amyloid plaques in the transgenic mice (Figure 3A) but not the age-matched controls (Figure 3B). Furthermore, we confirmed that the radioactive spots of [^{99m}Tc]BAT-Bp-2 corresponded with those of thioflavin-S staining in vitro in the same brain sections (Figure 3C), while there was no marked staining in the sections of wild-type mouse brain. The results suggest that [^{99m}Tc]BAT-Bp-2 had sufficient binding affinity to image β-amyloid plaques in vivo, although [^{99m}Tc]BAT-Bp-2 displayed lower affinity than [^{18}F]FPYBF-2.[21] However, some β-amyloid plaques, which were not labeled with [^{99m}Tc]BAT-Bp-2 in the brain sections, were also observed. This may be attributable to the lower brain uptake and lower affinity for β-amyloid plaques of [^{99m}Tc]BAT-Bp-2 than [^{18}F]FPYBF-2.

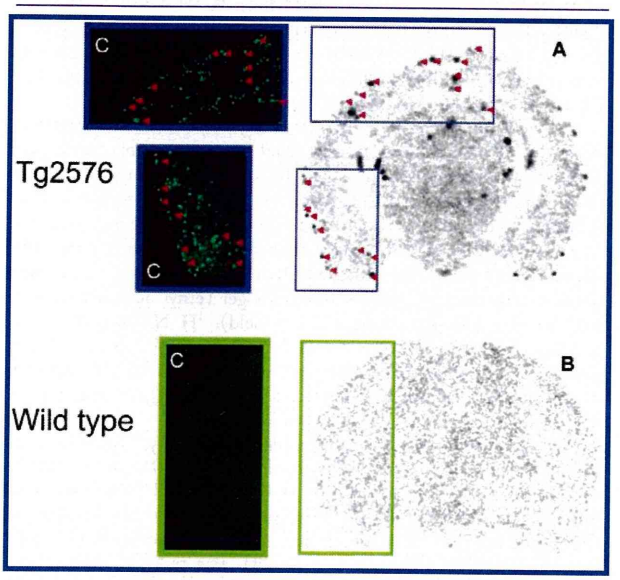

Figure 3. Labeling of β-amyloid plaques was visualized by autoradiography ex vivo with [^{99m}Tc]BAT-Bp-2 in brain sections of Tg2576 (A) and wild-type (B) mice. The same section was also stained with thioflavin-S (C), a pathological dye commonly used for staining β-amyloid plaques .

This is the first report that a ^{99m}Tc-labeled probe has successfully detected β-amyloid plaques in vivo. Therefore, [^{99m}Tc]BAT-Bp-2 should be investigated further as a potentially useful β-amyloid imaging probe.

■ CONCLUSION

In conclusion, three ^{99m}Tc-labeled pyridyl benzofuran derivatives and their corresponding rhenium complexes were successfully synthesized. All complexes showed affinity for Aβ in vitro and good uptake in the brain. Among them, [^{99m}Tc]BAT-Bp-2 not only displayed the highest initial uptake in the brain and a reasonable washout from the brain, but also showed extensive labeling of β-amyloid plaques in vivo. Taken together, [^{99m}Tc]BAT-Bp-2 may be a potential SPECT probe for imaging β-amyloid plaques in Alzheimer's brains.

■ EXPERIMENTAL SECTION

General Remarks. All chemicals used in synthesis were commercial products used without further purification. ^{1}H NMR spectra were obtained at 400 MHz on JEOL JNM-AL400 NMR spectrometers at room temperature with TMS as an internal standard. Chemical shifts are reported as δ values relative to the internal TMS. Coupling constants are reported in hertz. Multiplicity is defined by s (singlet), d (doublet), t (triplet), and m (multiplet). Mass spectra were acquired with a Shimadzu GC-MS-QP2010 Plus (ESI). HPLC was performed with a Shimadzu system (a LC-10AT pump with a SPD-10A UV detector, λ = 254 nm) with a Cosmosil C18 column (Nacalai Tesque, $5C_{18}$-AR-II, 4.6 mm × 150 mm) using a mobile phase (water/acetonitrile: 0 min 3/2 to 30 min 3/7) delivered at a flow rate of 1.0 mL/min. Fluorescent observation was performed by microscope (Nikon Eclipse 80i) with a BV-2A filter set (excitation, 400−440 nm; diachronic mirror, 455 nm; long pass filter, 470 nm). All key compounds were proven to show ≥99% purity by HPLC.

Chemistry. *5-(5-Methoxybenzofuran-2-yl)pyridin-2-amine (1).* A solution of 5-methoxybenzofuran-2-boronic acid (576 mg, 3.0 mmol), 2-amino-5-iodopyridine (660 mg, 3.0 mmol), and $Pd(Ph_3P)_4$ (366 mg, 0.3 mmol) in 2 M Na_2CO_3 (aq)/dioxane (1:1, 150 mL) was stirred overnight under reflux. The mixture was allowed to cool to room temperature, and 1 M NaOH (20 mL) was added. After extraction with ethyl acetate, the organic phase was dried over Na_2SO_4 and filtered. The filtrate was concentrated, and the residue was purified by silica gel chromatography (hexane:ethyl acetate = 1:1) to give 374 mg of **1** (52.1%). ^{1}H NMR (400 MHz, $CDCl_3$): δ 3.85 (s, 3H), 4.67 (s, 2H), 6.59 (d, 1H, J = 8.8 Hz), 6.76 (s, 1H), 6.82 (dd, 1H, J_1 = 8.8 Hz, J_2 = 2.4 Hz), 7.07 (d, 1H, J = 2.4 Hz), 7.36 (d, 1H, J = 8.8 Hz), 7.86 (dd, 1H, J_1 = 8.8 Hz, J_2 = 2.4 Hz), 8.67 (d, 1H, J = 2.4 Hz). MS: m/z 241 (M^+ + H).

2-(6-Aminopyridin-3-yl)benzofuran-5-ol (2). BBr_3 (8.0 mL, 1 M solution in CH_2Cl_2) was added to a solution of **1** (370 mg, 1.54 mmol) in CH_2Cl_2 (20 mL) dropwise in an ice bath. The mixture was allowed to warm to room temperature and stirred for 1 h. Water (20 mL) was added while the reaction mixture was cooled in an ice bath. After extraction with ethyl acetate, the organic phase was dried over Na_2SO_4 and filtered. The filtrate was concentrated, and the residue was purified by silica gel chromatography (hexane:ethyl acetate = 1:1) to give 221 mg of **2** (98.0%). ^{1}H NMR (400 MHz, $CDCl_3$): δ 4.67 (s, 2H), 6.59 (d, 1H, J = 8.8 Hz), 6.76 (s, 1H), 6.82 (dd, 1H, J_1 = 8.8 Hz, J_2 = 2.4 Hz), 7.07 (d, 1H, J = 2.4 Hz), 7.36 (d, 1H, J = 8.8 Hz), 7.86 (dd, 1H, J_1 = 8.8 Hz, J_2 = 2.4 Hz), 8.67 (d, 1H, J = 2.4 Hz). MS: m/z 227 (M^+ + H).

5-(5-Methoxybenzofuran-2-yl)-N-methylpyridin-2-amine (3). Sodium methoxide (275 mg, 5.0 mmol) was added to **1** (240 mg, 1.0 mmol) in methanol (15 mL) followed by paraformaldehyde (101 mg, 4.0 mmol). The solution was heated to reflux for 2 h and cooled to 0 °C with an ice bath. Sodium borohydride (128 mg, 4.0 mmol) was added. The reaction mixture was brought to reflux again for 1 h and poured onto crushed ice. After a standard workup with ethyl acetate,

the residue was purified by silica gel chromatography (hexane:ethyl acetate = 1:1) to give 234 mg of **3** (92.1%). ^{1}H NMR (400 MHz, $CDCl_3$): δ 2.98 (d, 3H, J = 5.2 Hz), 3.84 (s, 3H), 4.78 (s, 1H), 6.47 (d, 1H, J = 8.8 Hz), 6.76 (s, 1H), 6.84 (dd, 1H, J_1 = 8.8 Hz, J_2 = 4.4 Hz), 7.00 (d, 1H, J = 2.4 Hz), 7.36 (d, 1H, J = 8.4 Hz), 7.87 (dd, 1H, J_1 = 8.8 Hz, J_2 = 2.4 Hz), 8.59 (d, 1H, J = 2.8 Hz). MS: m/z 255 (M^+ + H).

*2-(6-(Methylamino)pyridin-3-yl)benzofuran-5-ol (**4**).* The same reaction as described above to prepare **2** was used, and 218 mg of **4** was obtained in a 99.0% yield from **3**. ^{1}H NMR (400 MHz, $CDCl_3$): δ 2.98 (d, 3H, J = 5.2 Hz), 4.78 (s, 1H), 6.47 (d, 1H, J = 8.8 Hz), 6.76 (s, 1H), 6.84 (dd, 1H, J_1 = 8.8 Hz, J_2 = 4.4 Hz), 7.00 (d, 1H, J = 2.4 Hz), 7.36 (d, 1H, J = 8.4 Hz), 7.87 (dd, 1H, J_1 = 8.8 Hz, J_2 = 2.4 Hz), 8.59 (d, 1H, J = 2.8 Hz). MS: m/z 241 (M^+ + H).

tert-Butyl 2-((3-Bromopropyl)(2-(tritylthio)ethyl)amino)ethyl (2-(tritylthio)ethyl)carbamate (TRT-Boc-BAT-Br). To a solution of TRT-Boc-BAT[18] (399.8 mg, 0.52 mmol) in CH_3CN (20 mL) were added K_2CO_3 (200 mg, 1.45 mmol) and 1,3-dibromopropane (110 μL, 1.0 mmol). The mixture was heated to reflux for 18 h, and after cooling to room temperature, evaporated dry. The residue was redissolved in $CHCl_3$ and washed with brine. The organic layers were dried with Na_2SO_4 and evaporated dry. The crude product was chromatographed on silica gel (ethyl acetate:hexane = 3:7) to give 244 mg of desired compound (53.0% yield). ^{1}H NMR (400 MHz, $CDCl_3$): δ 1.37 (s, 9H), 1.71–1.73 (m, 2H), 2.25–2.42 (m, 10H), 2.87–3.03 (m, 4H), 3.90–3.93 (m, 2H), 7.14–7.29 (m, 19H), 7.38–7.40 (m, 12H). MS: m/z 887 (M^+ + H).

*tert-Butyl 2-((3-(2-(6-Aminopyridin-3-yl)benzofuran-5-yloxy)propyl)(2-(tritylthio)ethyl)amino)ethyl(2-(tritylthio)ethyl)carbamate (**5**).* To a solution of **2** (18 mg, 0.08 mmol) and Boc-BAT-Br (70 mg, 0.08 mmol) in acetone (10 mL) was added cesium carbonate (31 mg, 0.10 mmol). The reaction mixture was heated to reflux for 5 h. After evaporation of the solvent, a saturated NaCl solution was added, and after extraction with $CHCl_3$, the organic layers were combined, dried with Na_2SO_4, and evaporated dry. The crude product was chromatographed on silica gel (ethyl acetate:hexane = 1:1) to give 62 mg of **5** (75.2% yield). ^{1}H NMR (400 MHz, $CDCl_3$): δ 1.37 (s, 9H), 1.71–1.73 (m, 2H), 2.25–2.42 (m, 10H), 2.87–3.03 (m, 4H), 3.90–3.93 (m, 2H), 4.80 (s, 2H), 6.55 (d, 1H, J = 8.8 Hz), 6.70 (s, 1H), 6.77 (dd, 1H, J_1 = 8.8 Hz, J_2 = 2.4 Hz), 6.95 (d, 1H, J = 2.8 Hz), 7.14–7.29 (m, 19H), 7.38–7.40 (m, 12H), 7.82 (J_1 = 8.8 Hz, J_2 = 2.4 Hz), 8.54 (d, 1H, J = 2.0 Hz). HRMS (FAB): m/z calcd for $C_{65}H_{66}N_4O_4S_2$ (M^+), 1030.4423; found, 1030.4417.

*Compound **6** (Re-BAT-Bp-1).* To a solution of **5** (25 mg, 0.02 mmol) in TFA (1 mL) was added triethylsilane (0.29 mL) and mixed for 10 min, and then the solvent was removed under a stream of nitrogen gas. The residue was resolved in 10 mL of CH_2Cl_2, $(Ph_3P)_2ReOCl_3$ (33 mg, 0.04 mmol), and 1 M sodium acetate in methanol (1 mL) was added. The reaction mixture was heated to reflux for 4 h. The mixture was filtered after cooling to room temperature. Evaporation of the solvent gave a residue which was purified with silica gel chromatography ($CHCl_3$:CH_3OH = 10:1), to give 6.1 mg of **6** (46.0% yield). ^{1}H NMR (400 MHz, $CDCl_3$): δ 2.27–2.34 (m, 2H), 2.98–3.06 (m, 2H), 3.28–3.47 (m, 2H), 3.78–3.93 (m, 2H), 4.07–4.33 (m, 6H), 6.56 (d, 1H, J = 8.8 Hz), 6.75 (s, 1H), 6.80 (d, 1H, J = 6.4 Hz), 6.98 (s, 1H), 7.36 (d, 1H, J = 8.8 Hz), 7.86 (d, 1H, J = 9.2 Hz), 8.65 (s, 1H). HRMS (FAB): m/z calcd for $C_{22}H_{28}N_4O_3ReS_2$ (M^+), 675.1471; found, 675.1469.

*tert-Butyl 2-((3-(2-(6-(Methylamino)pyridin-3-yl)benzofuran-5-yloxy)propyl)(2-(tritylthio)ethyl)amino)ethyl(2-(tritylthio)ethyl)-carbamate (**7**).* The same reaction as described above to prepare **5** was used, and 220.5 mg of **7** was obtained in a 70.3% yield from **4**. ^{1}H NMR (400 MHz, $CDCl_3$): δ 1.36 (s, 9H), 1.69–1.75 (m, 2H), 2.25–2.40 (m, 10H), 2.87–3.03 (m, 4H), 2.97 (s, 3H), 3.89–3.93 (m, 2H), 5.03 (s, 1H), 6.44 (d, 1H, J = 8.8 Hz), 6.68 (s, 1H), 6.76 (dd, 1H, J_1 = 8.8 Hz, J_2 = 2.4 Hz), 6.95 (d, 1H, J = 2.8 Hz), 7.14–7.25 (m, 19H), 7.38–7.39 (m, 12H), 7.85 (J_1 = 8.8 Hz, J_2 = 2.4 Hz), 8.56 (d, 1H, J = 2.0 Hz). HRMS (FAB): m/z calcd for $C_{66}H_{68}N_4O_4S_2$ (M^+), 1044.4580; found, 1044.4587.

*Compound **8** (Re-BAT-Bp-2).* The same reaction as described above to prepare **6** was used, and 30.1 mg of **8** was obtained in a 26.7% yield from **7**. ^{1}H NMR (400 MHz, $CDCl_3$): δ 2.27–2.34 (m, 2H), 2.97 (s, 3H), 2.98–3.06 (m, 2H), 3.28–3.47 (m, 2H), 3.78–3.93 (m, 2H), 4.07–4.33 (m, 6H), 6.56 (d, 1H, J = 8.8 Hz), 6.75 (s, 1H), 6.80 (d, 1H, J = 6.4 Hz), 6.98 (s, 1H), 7.36 (d, 1H, J = 8.8 Hz), 7.86 (d, 1H, J = 9.2 Hz), 8.65 (s, 1H). HRMS (FAB): m/z calcd for $C_{23}H_{30}N_4O_3ReS_2$ (M^+), 661.1314; found, 661.1312.

*5-(5-Methoxybenzofuran-2-yl)-N,N-dimethylpyridin-2-amine (**9**).* A mixture of **1** (360 mg, 1.5 mmol), paraformaldehyde (450 mg, 15 mmol), and sodium cyanoborohydride (284 mg, 4.5 mmol) in acetic acid (20 mL) was stirred at room temperature overnight and then poured into 100 mL of water. Sodium bicarbonate was added to adjust the pH to 8–9. After a standard workup with ethyl acetate, the residue was purified by silica gel chromatography (hexane:ethyl acetate = 3:1) to give 249 mg of **9** (62.0%). ^{1}H NMR (400 MHz, $CDCl_3$): δ 3.15 (s, 6H), 3.85 (s, 3H), 6.59 (d, 1H, J = 8.8 Hz), 6.76 (s, 1H), 6.82 (dd, 1H, J_1 = 8.8 Hz, J_2 = 2.4 Hz), 7.07 (d, 1H, J = 2.4 Hz), 7.36 (d, 1H, J = 8.8 Hz), 7.86 (dd, 1H, J_1 = 8.8 Hz, J_2 = 2.4 Hz), 8.67 (d, 1H, J = 2.4 Hz). MS: m/z 269 (M^+ + H).

*2-(6-(Dimethylamino)pyridin-3-yl)benzofuran-5-ol (**10**).* The same reaction as described above to prepare **2** was used, and 234 mg of **10** was obtained in a 98.9% yield from **9**. ^{1}H NMR (400 MHz, $CDCl_3$): δ 3.15 (s, 6H), 4.89 (s, 1H), 6.59 (d, 1H, J = 8.8 Hz), 6.76 (s, 1H), 6.82 (dd, 1H, J_1 = 8.8 Hz, J_2 = 2.4 Hz), 7.07 (d, 1H, J = 2.4 Hz), 7.36 (d, 1H, J = 8.8 Hz), 7.86 (dd, 1H, J_1 = 8.8 Hz, J_2 = 2.4 Hz), 8.67 (d, 1H, J = 2.4 Hz). MS: m/z 255 (M^+ + H).

*5-(5-(3-Bromopropoxy)benzofuran-2-yl)-N,N-dimethylpyridin-2-amine (**11**).* To a solution of **10** (324.9 mg, 1.27 mmol) in CH_3CN (20 mL) were added K_2CO_3 (216 mg, 1.57 mmol) and 1,3-dibromopropane (0.65 mL, 6.4 mmol). The mixture was heated to reflux for 18 h, and after cooling to room temperature, evaporated dry. The residue was redissolved in $CHCl_3$ and washed with brine. The organic layers were dried with Na_2SO_4 and evaporated dry. The crude product was chromatographed on silica gel (ethyl acetate:hexane = 3:7) to give 275 mg of **11** (73.2% yield). ^{1}H NMR (400 MHz, $CDCl_3$): δ 2.09 (t, 2H, J = 6.4 Hz), 3.09 (s, 6H), 3.60(t, 2H, J = 6.4 Hz), 4.08 (t, 2H, J = 5.8 Hz), 6.48 (s, 1H), 6.68 (s, 1H), 6.80 (d, 1H, J = 6.4 Hz), 6.96 (s, 1H), 7.33 (d, 1H, J = 8.8 Hz), 7.79 (d, 1H, J = 9.2 Hz), 8.64 (s, 1H). MS: m/z 375 (M^+ + H).

*tert-Butyl-2-((3-(2-(6-(dimethylamino)pyridin-3-yl)benzofuran-6-yloxy)propyl)(2-(tritylthio)ethyl)amino)ethyl(2-(tritylthio)ethyl)-carbamate (**12**).* To a solution of **11** (272 mg, 0.72 mmol) and *tert*-butyl 2-(tritylthio)ethyl(2-(2-(tritylthio)ethylamino)ethyl)carbamate (TRT-Boc-BAT)[18] (550 mg, 0.72 mmol) in acetonitrile (30 mL) was added DIPEA (225 μL, 1.45 mmol). The reaction mixture was heated to reflux for 12 h. When the solvent had evaporated, a saturated NaCl solution was added, and after extraction with $CHCl_3$, the organic layers were combined, dried with Na_2SO_4, and evaporated dry. The crude product was chromatographed on silica gel (ethyl acetate:hexane = 3:7) to give 343.6 mg of **12** (45.0% yield). ^{1}H NMR (400 MHz, $CDCl_3$): δ 1.26 (s, 9H), 1.61 (s, 2H), 2.16–2.30 (m, 10H), 2.77–2.87 (m, 4H), 2.97 (s, 6H), 3.81 (s, 2H), 6.40 (d, 1H, J = 9.2 Hz), 6.55 (s, 1H), 6.66 (d, 1H, J = 6.4 Hz), 6.84 (s, 1H), 7.03–7.20 (m, 19H), 7.21–7.31 (m, 12H), 7.71 (d, 1H, J = 9.2 Hz), 8.55 (s, 1H). HRMS (FAB): m/z calcd for $C_{67}H_{71}N_4O_4S_2$ (M^+), 1059.4917; found, 1059.4910.

*Compound **13** (Re-BAT-Bp-3).* The same reaction as described above to prepare **6** was used, and 29 mg of **13** was obtained in a 33.0% yield from **12**. ^{1}H NMR (400 MHz, $CDCl_3$): δ 2.27–2.34 (m, 2H), 2.98–3.06 (m, 2H), 3.16 (s, 6H), 3.28–3.47 (m, 2H), 3.78–3.93 (m, 2H), 4.07–4.33 (m, 6H), 6.56 (d, 1H, J = 8.8 Hz), 6.75 (s, 1H), 6.80 (d, 1H, J = 6.4 Hz), 6.98 (s, 1H), 7.36 (d, 1H, J = 8.8 Hz), 7.86 (d, 1H, J = 9.2 Hz), 8.65 (s, 1H). HRMS (FAB): m/z calcd for $C_{24}H_{32}N_4O_3ReS_2$ (M^+), 675.1471; found, 675.1469.

Binding Assays Using the Aggregated Aβ Peptides in Solution. Aβ(1–42) was purchased from Peptide Institute (Osaka, Japan). Aggregation was carried out by gently dissolving the peptide (0.25 mg/mL) in a buffer solution (pH 7.4) containing 10 mM sodium phosphate and 1 mM EDTA. The solution was incubated at 37 °C for 42 h with gentle and constant shaking. A mixture containing 50 μL of Re complex (**6**, **8**, or **13**) (10^{-5}–10^{-10} M in 10% EtOH),

50 μL of [^{125}I] IMPY (50000−100000 cpm), 50 μL of Aβ(1−42) aggregates (28 nM), and 850 μL of 10% EtOH was incubated at room temperature for 3 h. The mixture was then filtered through Whatman GF/B filters using a Brandel M-24 cell harvester, and the radioactivity of the filters containing the bound ^{125}I ligand was measured in a γ counter. Values for the half-maximal inhibitory concentration (IC_{50}) were determined from displacement curves of three independent experiments using GraphPad Prism 5.0, and those for the inhibition constant (K_i) were calculated using the Cheng−Prusoff equation: $K_i = IC_{50}/(1 + [L]/K_d)$, where [L] is the concentration of [^{125}I]IMPY used in the assay and K_d is the dissociation constant of IMPY.

^{99m}Tc Labeling Reaction and Analysis by RP-HPLC. To a solution of sodium heptonate dehydrate (2 g, 7.04 mmol) in nanopure water (25 mL) was added 0.75 mL of a $SnCl_2{\cdot}2H_2O$ solution [12 mg of Tin(II) chloride dehydrate (53.2 mmol) dissolved in 15 mL of 0.1 M HCl]. This solution was adjusted to pH 8.5−9.0 using a small amount of 0.1 M NaOH and then lyophilized to give Sn glucoheptonate (SnGH) kit. SnGH kit (1 mg) was added to a $Na^{99m}TcO_4$ solution (200 μL) and reacted at room temperature for 10 min to give a ^{99m}TcGH solution. To a solution of precursor (**5**, **7**, or **12**) (0.5 mg) in TFA (200 μL) was mixed in triethylsilane (10 μL), and the solvents were removed under a stream of nitrogen gas. The residue was resolved in acetonitrile (200 μL), followed by addition of 0.1 M HCl (15 μL) and the ^{99m}TcGH solution (200 μL). The reaction mixture was heated to 85 °C for 20 min. After cooling to room temperature, sodium bicarbonate was added to adjust the pH to 8−9. The mixture was purified with RP-HPLC. The ^{99m}Tc-labeled pyridyl benzofuran complex was analyzed by analytical RP-HPLC on a Cosmosil C_{18} column ($5C_{18}$-AR-II, 4.6 mm × 150 mm) with a solvent of H_2O/acetonitrile (0 min 3/2 to 30 min 3/7) at a flow rate of 1.0 mL/min. The absorption of the complexes was measured at 254 nm, and the radioactivity of the ^{99m}Tc-labeled form was recorded for 60 min.

log *P* Measurement. The experimental determination of partition coefficients was performed in 1-octanol and PBS buffer (pH 7.4). The two phases were presaturated with each other. 1-Octanol (3.0 mL) and PBS (3.0 mL) were pipetted into a 12 mL test tube containing 1.11 MBq of [^{99m}Tc]tracer. The test tube was vortexed for 2 min and centrifuged (5 min, 1000*g*). Aliquots (500 μL) from the 1-octanol and PBS phases were transferred into two test tubes for counting. One milliliter of the remaining 1-octanol phase was transferred into a new test tube. New 1-octanol (2.0 mL) and PBS (3.0 mL) were pipetted into the same test tube. The vortexing, centrifuging, and counting were repeated. The amount of radioactivity in each tube was measured with a γ counter and corrected for decay. The partition coefficient was calculated using the equation: $\log P = \log[\text{count}_{1\text{-octanol}}/\text{count}_{PBS}]$

Biodistribution in Normal Mice. Experiments with animals were conducted in accordance with our institutional guidelines and approved by the Kyoto University Animal Care Committee. While under isoflurane anesthesia, ddY mice (5 weeks old, 22−25 g, male) were injected intravenously with 100 μL of a 10% ethanol in saline solution containing [^{99m}Tc]tracers (148 kBq) via the tail. The mice (n = 5 for each time point) were sacrificed at 2, 10, 30, and 60 min postinjection. The organs of interest were removed and weighed, and radioactivity was measured with an automatic γ counter (COBRAII, Packard). The percent dose per organ was calculated by comparing the tissue counts with suitably diluted aliquots of the injected material. The %dose/g of samples was calculated by comparing the sample counts with the count for the diluted initial dose.

Ex Vivo Autoradiography Using Tg2576 Mice. Tg2576 transgenic mice (27 months, male) and wild-type mice (27 months, male) were used as an Alzheimer's model and an age-matched control, respectively. After anesthetization with 1% isoflurane, 16.6 MBq of [^{99m}Tc]BAT-Bp-2 in 250 μL of a 10% ethanol solution was injected through the tail. The animals were allowed to recover for 30 min and then killed by decapitation. The brains were immediately removed and frozen in a dry ice/hexane bath. Sections of 20 μm were cut and exposed to a BAS imaging plate (Fuji Film, Tokyo, Japan) overnight. Ex vivo film autoradiograms were thus obtained. After autoradiographic examination, the same sections were stained by thioflavin-S to confirm the presence of β-amyloid plaques. For the staining of thioflavin-S, sections were immersed in a 0.125% thioflavin-S solution containing 50% EtOH for 5 min and washed in 50% EtOH. After drying, the sections were examined using a microscope (Nikon, Eclipse 80i) equipped with a B-2A filter set (excitation, 450−490 nm; diachronic mirror, 505 nm; long-pass filter, 520 nm).

■ AUTHOR INFORMATION

Corresponding Author

*Phone: +81-75-753-4608. Fax: +81-75-753-4568. E-mail: ono@pharm.kyoto-u.ac.jp.

Notes

The authors declare no competing financial interest.

■ ACKNOWLEDGMENTS

The study was supported by the Funding Program for Next Generation World-Leading Researchers (NEXT Program), and a Grant-in-Aid for Young Scientists (A) and Exploratory Research from the Ministry of Education, Culture, Sports, Science, and Technology, Japan.

■ ABBREVIATIONS USED

AD, Alzheimer's disease; SP, senile plaque; NFT, neurofibrillary tangle; Aβ, β-amyloid peptide; PET, positron emission tomography; SPECT, single photon emission computed tomography; MCI, mild cognitive impairment; BAT, bis(aminoethanethiol); BBB, blood−brain barrier; GH, glucoheptonate; PIB, 2-(4′-(methylaminophenyl)-6-hydroxybenzothiazole; IMPY, 6-iodo-2-(4′-dimethylamino)phenyl-imidazo[1,2-*a*]pyridine

■ REFERENCES

(1) Mathis, C. A.; Wang, Y.; Klunk, W. E. Imaging β-amyloid plaques and neurofibrillary tangles in the aging human brain. *Curr. Pharm. Des.* **2004**, *10*, 1469−1492.

(2) Glenner, G. G.; Wong, C. W. Alzheimer's disease and Down's syndrome: sharing of a unique cerebrovascular amyloid fibril protein. *Biochem. Biophys. Res. Commun.* **1984**, *122*, 1131−1135.

(3) Selkoe, D. J. Alzheimer's disease: genes, proteins, and therapy. *Physiol. Rev.* **2001**, *81*, 741−766.

(4) Ono, M.; Wilson, A.; Nobrega, J.; Westaway, D.; Verhoeff, P.; Zhuang, Z. P.; Kung, M. P.; Kung, H. F. ^{11}C-labeled stilbene derivatives as Aβ-aggregate-specific PET imaging agents for Alzheimer's disease. *Nucl. Med. Biol.* **2003**, *30*, 565−571.

(5) Verhoeff, N. P.; Wilson, A. A.; Takeshita, S.; Trop, L.; Hussey, D.; Singh, K.; Kung, H. F.; Kung, M. P.; Houle, S. In vivo imaging of Alzheimer disease β-amyloid with [^{11}C]SB-13 PET. *Am. J. Geriatr. Psychiatry* **2004**, *12*, 584−595.

(6) Mathis, C. A.; Wang, Y.; Holt, D. P.; Huang, G. F.; Debnath, M. L.; Klunk, W. E. Synthesis and evaluation of ^{11}C-labeled 6-substituted 2-arylbenzothiazoles as amyloid imaging agents. *J. Med. Chem.* **2003**, *46*, 2740−2754.

(7) Klunk, W. E.; Engler, H.; Nordberg, A.; Wang, Y. B., G.; Holt, D. P.; Bergstrom, M.; Savitcheva, I.; Huang, G. F.; Estrada, S.; Ausen, B.; Debnath, M. L.; Barletta, J.; Price, J. C.; Sandell, J.; Lopresti, B. J.; Wall, A.; Koivisto, P.; Antoni, G.; Mathis, C. A.; Langstrom, B. Imaging brain amyloid in Alzheimer's disease with Pittsburgh compound-B. *Ann. Neurol.* **2004**, *55*, 306−319.

(8) Koole, M.; Lewis, D. M.; Buckley, C.; Nelissen, N.; Vandenbulcke, M.; Brooks, D. J.; Vandenberghe, R.; Van Laere, K. Whole-body biodistribution and radiation dosimetry of ^{18}F-GE067: a radioligand for in vivo brain amyloid imaging. *J. Nucl. Med.* **2009**, *50*, 818−822.

(9) Villemagne, V. L.; Ong, K.; Mulligan, R. S.; Holl, G.; Pejoska, S.; Jones, G.; O'Keefe, G.; Ackerman, U.; Tochon-Danguy, H.; Chan, J. G.; Reininger, C. B.; Fels, L.; Putz, B.; Rohde, B.; Masters, C. L.;

Rowe, C. C. Amyloid imaging with [^{18}F]florbetaben in Alzheimer disease and other dementias. *J. Nucl. Med.* **2011**, *52*, 1210−1217.
(10) Lin, K. J.; Hsu, W. C.; Hsiao, I. T.; Wey, S. P.; Jin, L. W.; Skovronsky, D.; Wai, Y. Y.; Chang, H. P.; Lo, C. W.; Yao, C. H.; Yen, T. C.; Kung, M. P. Whole-body biodistribution and brain PET imaging with [^{18}F]AV-45, a novel amyloid imaging agent—a pilot study. *Nucl. Med. Biol.* **2010**, *37*, 497−508.
(11) Choi, S. R.; Golding, G.; Zhuang, Z. P.; Zhang, W.; Lim, N.; Hefti, F.; Benedum, T. E.; Kilbourn, M. R.; Skovronsky, D.; Kung, H. F. Preclinical properties of ^{18}F-AV-45: a PET agent for Aβ plaques in the brain. *J. Nucl. Med.* **2009**, *50*, 1887−1894.
(12) Zhen, W.; Han, H.; Anguiano, M.; Lemere, C. A.; Cho, C. G.; Lansbury, P. T. J. Synthesis and amyloid binding properties of rhenium complexes: preliminary progress toward a reagent for SPECT imaging of Alzheimer's disease brain. *J. Med. Chem.* **1999**, *42*, 2805−2815.
(13) Dezutter, N. A.; Dom, R. J.; de Groot, T. J.; Bormans, G. M.; Verbruggen, A. M. ^{99m}Tc-MAMA-chrysamine G, a probe for β-amyloid protein of Alzheimer's disease. *Eur. J. Nucl. Med.* **1999**, *26*, 1392−1399.
(14) Zhuang, Z. P.; Kung, M. P.; Hou, C.; Ploessl, K.; Kung, H. F. Biphenyls labeled with technetium 99m for imaging β-amyloid plaques in the brain. *Nucl. Med. Biol.* **2005**, *32*, 171−184.
(15) Serdons, K.; Verduyckt, T.; Cleynhens, J.; Terwinghe, C.; Mortelmans, L.; Bormans, G.; Verbruggen, A. Synthesis and evaluation of a [^{99m}Tc]-BAT-phenylbenzothiazole conjugate as a potential in vivo tracer for visualization of amyloid β. *Bioorg. Med. Chem. Lett.* **2007**, *17*, 6086−6090.
(16) Ono, M.; Ikeoka, R.; Watanabe, H.; Kimura, H.; Fuchigami, T.; Haratake, M.; Saji, H.; Nakayama, M. Synthesis and evaluation of novel chalcone derivatives with ^{99m}Tc/Re complexes as potential probes for detection of β-amyloid plaques. *ACS Chem. Neurosci.* **2010**, *1*, 598.
(17) Ono, M.; Ikeoka, R.; Watanabe, H.; Kimura, H.; Fuchigami, T.; Haratake, M.; Saji, H.; Nakayama, M. ^{99m}Tc/Re complexes based on flavone and aurone as SPECT probes for imaging cerebral β-amyloid plaques. *Bioorg. Med. Chem. Lett.* **2010**, *20*, 5743−5748.
(18) Sagnou, M.; Benaki, D.; Triantis, C.; Tsotakos, T.; Psycharis, V.; Raptopoulou, C. P.; Pirmettis, I.; Papadopoulos, M.; Pelecanou, M. Curcumin as the OO bidentate ligand in "2 + 1" complexes with the $[M(CO)_3]^+$ (M = Re, ^{99m}Tc) tricarbonyl core for radiodiagnostic applications. *Inorg. Chem.* **2011**, *50*, 1295−1303.
(19) Cheng, Y.; Ono, M.; Kimura, H.; Kagawa, S.; Nishii, R.; Kawashima, H.; Saji, H. Fluorinated benzofuran derivatives for PET imaging of β-amyloid plaques in Alzheimer's disease brains. *ACS Med. Chem. Lett.* **2010**, *1*, 321−325.
(20) Cheng, Y.; Ono, M.; Kimura, H.; Kagawa, S.; Nishii, R.; Saji, H. A novel ^{18}F-labeled pyridyl benzofuran derivative for imaging of β-amyloid plaques in Alzheimer's brains. *Bioorg. Med. Chem. Lett.* **2010**, *20*, 6141−6144.
(21) Ono, M.; Cheng, Y.; Kimura, H.; Cui, M.; Kagawa, S.; Nishii, R.; Saji, H. Novel ^{18}F-labeled benzofuran derivatives with improved properties for positron emission tomography (PET) imaging of β-amyloid plaques in Alzheimer's brains. *J. Med. Chem.* **2011**, *54*, 2971−2979.
(22) Oya, S.; Plössl, K.; Kung, M. P.; Stevenson, D. A.; Kung, H. F. Small and neutral Tc(^{V})O BAT, bisaminoethanethiol (N_2S_2) complexes for developing new brain imaging agents. *Nucl. Med. Biol.* **1998**, *25*, 135−140.
(23) Miyaura, N.; Yamada, K.; Suzuki, A. A new stereospecific crosscoupling by the palladium-catalyzed reaction of 1-alkenylboranes with 1-alkenyl or 1-alkynyl halides. *Tetrahedron Lett.* **1979**, *36*, 3437−3440.
(24) Ono, M.; Kawashima, H.; Nonaka, A.; Kawai, T.; Haratake, M.; Mori, H.; Kung, M. P.; Kung, H. F.; Saji, H.; Nakayama, M. Novel benzofuran derivatives for PET imaging of β-amyloid plaques in Alzheimer's disease brains. *J. Med. Chem.* **2006**, *49*, 2725−2730.
(25) Zhang, W.; Oya, S.; Kung, M. P.; Hou, C.; Maier, D. L.; Kung, H. F. F-18 stilbenes as PET imaging agents for detecting β-amyloid plaques in the brain. *J. Med. Chem.* **2005**, *48*, 5980−5988.
(26) Ono, M.; Fuchi, Y.; Fuchigami, T.; Kobashi, N.; Kimura, H.; Haratake, M.; Saji, H.; Nakayama, M. Novel benzofurans with ^{99m}Tc complexes as probes for imaging cerebral β-amyloid plaques. *ACS Med. Chem. Lett.* **2010**, *1*, 443−447.
(27) Meltzer, P. C.; Blundell, P.; Jones, A. G.; Mahmood, A.; Garada, B.; Zimmerman, R. E.; Davison, A.; Holman, B. L.; Madras, B. K. A technetium-99m SPECT imaging agent which targets the dopamine transporter in primate brain. *J. Med. Chem.* **1997**, *40*, 1835−1844.
(28) Francesconi, L. C.; Graczyk, G.; Wehrli, S.; Shaikh, S. N.; McClinton, D.; Liu, S.; Zubieta, J.; Kung, H. F. Synthesis and characterization of neutral MVO (M = technetium, rhenium) amine-thiol complexes containing a pendant phenylpiperidine group. *Inorg. Chem.* **1993**, *32*, 3114−4124.
(29) O'Neil, J. P.; Wilson, S. R.; Katzenellenbogen, J. A. Preparation and structural characterization of monoamine-monoamide bis(thiol) oxo complexes of technetium(V) and rhenium(V). *Inorg. Chem.* **1994**, *33*, 319−323.
(30) Bartholomä, M. D.; Louie, A. S.; Valliant, J. F.; Zubieta, J. Technetium and gallium derived radiopharmaceuticals: comparing and contrasting the chemistry of two important radiometals for the molecular imaging era. *Chem. Rev.* **2010**, *110*, 2903−2920.
(31) Ono, M.; Haratake, M.; Saji, H.; Nakayama, M. Development of novel β-amyloid probes based on 3,5-diphenyl-1,2,4-oxadiazole. *Bioorg. Med. Chem. Lett.* **2008**, *16*, 6867−6872.
(32) Watanabe, H.; Ono, M.; Ikeoka, R.; Haratake, M.; Saji, H.; Nakayama, M. Synthesis and biological evaluation of radioiodinated 2,5-diphenyl-1,3,4-oxadiazoles for detecting β-amyloid plaques in the brain. *Bioorg. Med. Chem. Lett.* **2009**, *17*, 6402−6406.
(33) Ono, M.; Yoshida, N.; Ishibashi, K.; Haratake, M.; Arano, Y.; Mori, H.; Nakayama, M. Radioiodinated flavones for in vivo imaging of β-amyloid plaques in the brain. *J. Med. Chem.* **2005**, *48*, 7253−7260.
(34) Ono, M.; Maya, Y.; Haratake, M.; M., N. Synthesis and characterization of styrylchromone derivatives as β-amyloid imaging agents. *Bioorg. Med. Chem.* **2007**, *15*, 444−450.
(35) Ono, M.; Haratake, M.; Mori, H.; Nakayama, M. Novel chalcones as probes for in vivo imaging of β-amyloid plaques in Alzheimer's brains. *Bioorg. Med. Chem.* **2007**, *15*, 6802−6809.
(36) Cui, M.; Ono, M.; Kimura, H.; Liu, B.; Saji, H. Novel quinoxaline derivatives for in vivo imaging of β-amyloid plaques in the brain. *Bioorg. Med. Chem. Lett.* **2011**, *21*, 4193−4196.
(37) Kung, M. P.; Hou, C.; Zhuang, Z. P.; Cross, A. J.; Maier, D. L.; Kung, H. F. Characterization of IMPY as a potential imaging agent for β-amyloid plaques in double transgenic PSAPP mice. *Eur. J. Nucl. Med. Mol. Imaging* **2004**, *31*, 1136−1145.
(38) Kung, M. P.; Hou, C.; Zhuang, Z. P.; Zhang, B.; Skovronsky, D.; Trojanowski, J. Q.; Lee, V. M.; Kung, H. F. IMPY: an improved thioflavin-T derivative for in vivo labeling of β-amyloid plaques. *Brain Res.* **2002**, *956*, 202−210.
(39) Hsiao, K.; Chapman, P.; Nilsen, S.; Eckman, C.; Harigaya, Y.; Younkin, S.; Yang, F.; Cole, G. Correlative memory deficits, Aβ elevation, and amyloid plaques in transgenic mice. *Science* **1996**, *274*, 99−103.